10.5194/amt-2020-319 Revisions

Shoma Yamanouchi et al.

General Revisions:

We thank the two reviewers for their helpful comments, which have enabled us to improve the manuscript. The reviewers' comments are in regular font below and our responses are in bold font. Line numbers in the responses refer to the revised manuscript with changes tracked. Also of note is that there was a minor bug in the trend analysis code; this was revised, and affected values were corrected (this only affected the 2σ confidence intervals from bootstrap resampling).

Reviewer 1

The approach to determine the observational footprint of the FTIR column measurements seems to be oversimplified. It is only based in correlating the data with the satellite observations at different spatial and temporal scales. The best correlation and slope is obtained with the most strict criteria (25km/20 min). A proper footprint analysis would require to take the wind fields within the considered time period in consideration, which is not done. Although this simple analysis gives some indication of the representativeness of ground-based measurement, it should not be claimed in the text that a proper observational footprint assessment has been performed.

All sentences claiming that the "footprint assessment" was performed were replaced by sentences that mention the representativeness of ground-based measurements.

A bias would be expected to be observed between the FTIR and in situ data just because the FTIR only measures during sunny conditions. NAPS data is collected regularly every third day. Moreover, NH3 has a strong diurnal pattern that is not reported in this paper. While in situ data represents the average concentration within a 24 h period, FTIR data is available only during the day.

A brief discussion of this bias was added (Line 248).

The authors contrast the trends from the linear regressions from both data sets (TAO and NAPS) when outliers are and are not considered (L204). However, no mention or explanation is given for this source of bias given that NH3 concentrations are probably expected to peak during warmer days and warmer hours. It would be interesting to compare both data sets only for coincident

measurement days and give a more comprehensive explanation of this additional source of bias.

The comparison analysis using only coincident measurements is shown in Figure 5a. A brief discussion on warmer days and higher NH_3 was added, along with an additional analysis to examine coincident FTIR and in-situ measurements and temperatures; on three occasions where simultaneous enhancements were observed in the FTIR and in-situ data (once in May 2014, twice in May 2016), the daily average temperatures were higher than the monthly averages (Line 248-259).

It seems that the comparison of both TAO and IASI data sets with GEOS-Chem is challenging due to the coarse resolution of the model. It is shown from the comparison of the ground-based data with the satellite observations that NH3 presents high frequency variability in the region. It would then seem logical that the authors filter out the enhancements from the FTIR data, as done in the trend analysis, before correlating to the model data. The same could apply to IASI data since the enhancements observed within the large model domain are probably due to local emissions that are not well represented by the model. Figures 9a and b could then show the correlation and regression results as is, as well as from the filtered data sets.

This analysis was performed. Filtered FTIR measurements compared with GEOS-Chem resulted in r^2 = 0.22 and slope = 0.68 (when no filtering was performed, the values were r^2 = 0.26 and slope = 1.16). Comparisons of filtered IASI observations and GEOS-Chem resulted in r^2 = 0.29 and slope = 0.57 (when no filtering was performed, the values were r^2 = 0.33 and slope = 0.85). Corresponding plots were added (Figures 9c and 9d).

L28. The sentence is not accurate. The health impact of PM2.5 is strongly dependent on the chemical composition and the cited study does not take composition into account. In the context of this contribution, the PM containing ammonium salts are not the most hazardous and also those that contribute to smog are rather organic in nature. Please rephrase.

The sentence was reworded and another reference added here (Schiferl et al., 2014). We are not claiming that particulate matter forming due to ammonium salts are the most hazardous. Additionally, recent studies (e.g., Liu et al., 2019; Wielgosiński & Czerwińska, 2020) have shown that ammonium salts do contribute to smog as well as haze. The sentence was also reworded clarify this (Line 29-34).

L41. Referring to NH3 being injected to the free troposphere, you may want to cite Hoepfner et al 2016 (www.atmos-chem-phys.net/16/14357/2016/)

The reference was added (Line 48).

L86. A citation or description for the camera and solar disk-fitting system of the solar tracker is missing.

Further details can be found in Franklin (2015, http://hdl.handle.net/10222/64642). This reference was added.

L90 Should say "… microwindows in the … and … spectral regions."

Fixed (Line 98-99).

L76. Was there any quality control and data filtering performed? Please describe. Same for the in situ data.

No filtering was done for the in-situ (NAPS) data, although all NAPS sites adhere to quality control/quality assurance guidelines set forth by the Canadian Council of Ministers of the Environment (see https://www.ccme.ca/files/Resources/air/Ambient%20Air%20Monitoring%20and%20QA-QC%20Guidelines_en%20SECURE.pdf for details). FTIR columns were retrieved to conform to NDACC standards. Archived species are filtered by RMS/DOFS ratio.

L110. No need to repeat (National Air Pollution Surveillance Program)

The repeated bit was a part of the citation for the data (link to an entry references section). This has been removed (Line 119).

L117. Define the IASI acronym.

This was previously defined in the introduction (Line 73).

L121. May not be clear to the reader what a 2 x 2 circular pixel is. Maybe a matrix of 2 x 2 pixels?

The sentence was replaced with "[a]t nadir, the field of view is a 2 x 2 matrix of pixels, each with a 12 km diameter (Clerbaux et al., 2009)" (Line 132-133).

L126. Indicate the overpass times of each satellite instrument

The 3 IASI instruments are onboard the Metop A, B and C satellites which are all in the same polar orbit. Measurements are then performed at 09:30 and 21:30 mean local solar time for the descending and ascending orbits. A sentence clarifying this was added (Line 128-130).

L155 What do "longer time series" refer to? The length considered in this contribution? Please specify.

This refers to the duration of the measured dataset. In the method outlined by Weatherhead et al. (1998), measurements that are highly auto-correlated require longer time periods to obtain trends (for any given confidence interval).

L165. If mirroring a value is the same as taking its absolute value, the readers might be more familiar with the second terminology. It may also be wise to mention that the average of the mirrored residuals include the positive ones.

The term "mirroring" was used here, as it was also used by Zellweger et al. (2009). The argument for using this terminology is that the residuals should have both negative and positive terms, and in this analysis, the positive ones were "replaced" by the absolute values of the negative ones. The positive residuals are not used, in order to reduce biases introduced by enhancements.

Fig4. Figure 4 b) seems redundant since no additional information is provided with respect to a).

This figure was included to better illustrate points made around line 237.

Fig5. It would seem sufficient to show the correlation plots a) and e) in this figure, while keeping the results of the different resampling periods in the text (L219-223) L300. A larger trend with outliers with respect to that obtained without them may not be conclusive when looking at the data availability of the TOA data series. Measurements seem to be performed more regularly in recent years so to me the increase in seasonal variability is more evident when comparing for example the standard deviations year to year.

The standard deviations of the TAO columns are in fact increasing (as discussed in Section 3.1). The conclusion was edited to re-iterate this point (Line 338).

Reviewer 2

General Comments:

Why was the nested version of GEOS-Chem over North America not used? It includes Toronto in the domain and is at finer resolution (0.25°′ 0.3125°) than the global domain.

The nested model would be very computationally expensive to run given the long time series. In addition, the amount of storage space required to archive all of the meteorological fields at high resolution for the whole observational record is also a limiting factor. Given that the focus of the paper is the long time series of NH_3 observations, we believe that using a model that could be run over the entire time series was more appropriate.

There is quite a lot of information relevant to model representation of NH3 that is missing in the model description section. These include the following: The inventories used in the model to represent US and Canadian SO2 and NO_X sources that form sulfate and nitrate that influence NH3 uptake to aerosols. The version of EDGAR and whether this is the inventory that represents anthropogenic NH3 emissions over the domain of interest or whether it is a combination of EDGAR and GEIA (now quite outdated and only really used in the model to represent natural NH3 emissions). The base year of each inventory. Whether annual scaling factors are applied to any of the emissions that would have declined due to emission regulations (typically NO_X and SO2). Whether seasonal scaling factors are applied to NH3 emissions in the model.

EDGAR v4.2 and GEIA were used as global inventories, with GEIA providing the natural source of NH_3. The global inventories were replaced with the US EPA National Emission Inventory for 2011 (NEI11) in the United States, and by the Criteria Air Contaminants (CAC) from the National Pollutant Release Inventory in Canada. The NEI11 emissions were scaled between the years 2006–2013, whereas the CAC NH_3 emissions used 2008 as the base year, with no scaling applied. The NEI11 emissions were hourly, whereas the CAC emissions are monthly.

The information above was added to the manuscript in Section 2.4.

The model also seems to be underutilised to provide context for the study region. The inventories could, for example, be used to assess the relative proportion of vehicular, agricultural, and natural emissions to total NH3 emissions and to determine the role of changes in sulfate and nitrate (due to emission regulations of SO2 and NO_X sources) on observed trends in NH3.

We agree that this would be a good use of the model. However, to effectively attribute the observed change in $NH_3$to vehicular, agricultural, or other emission sources would require use of the nested model, and as we noted in our previous response it is not computationally feasible to run the nested model over the whole observational record. This suggestion would be a valuable follow-up study, focusing on a limited period of the record (e.g., one or two years). Our focus in this manuscript is on the long time series of the FTIR measurements.

What is the fit that is applied to the data to obtain the trends? And what is the determination of significance? It is stated in the text that "The number of years of measurements needed for the trend to be statistically (2s) significant was found to be 33.8 years and 29.3 years" (p. 6, lines 177-178), but it is not clear why this is the case given that the 2s uncertainty is much less than the trend value. An explicit statement of what the authors use as a significance criterion might help avoid confusion.

The fit used in this study was a trended Fourier series of order 3. This is discussed in Section 2.6. Two different statistical analysis methods were used in this study. The uncertainties given for each values were obtained using bootstrapping, and the "number of years of measurements needed for the trend to be statistically significant" was estimated using a method outlined by Weatherhead et al., (1998). This method has several drawbacks when used with data with irregular measurement intervals, as is the case for FTIR. This is discussed in the Section 2.6.

The FTIR instrument and measurements are referred to in figures/tables/text as FTIR, TAO, or TAO FTIR. To avoid confusion, stick with one of these throughout.

Most of the references to the ground-based FTIR were consolidated to simply "FTIR." However, in some sections (especially sections where IASI is mentioned, e.g., Sections 2.3, 2.5, 3.3, 4), the term "TAO FTIR" was used to avoid confusion, as IASI is also an FTIR spectrometer instrument. "TAO FTIR" was also used in places where NDACC, and/or other FTIRs were mentioned. It should also be mentioned that TAO is home to several instruments, including the FTIR. Additionally, in places where the *location* of the FTIR is mentioned (e.g., Figure 7 caption), term TAO was used.

Specific Comments:

p1, line 14: There is no context for the use of "resampling" in the abstract to be able to follow what this implies for the results obtained. What is being resampled? And why does it alter the correlation?

"Resampling" was changed to "averaging" to avoid confusion (Line 14).

p2, line 38: Briefly elaborate on the link between NH_3 concentrations and SO_2 and NO_X emissions.

Sentence clarifying this was added (Line 42-44).

p2, line 39: "...as well as by reactions with acids in the atmosphere" sounds like it is happening in the gas phase. Make clear that this is a heterogeneous process.

"[H]eterogeneous" was added to make this clear (Line 43).

p3, line 59: What is the NH_3 source from greenery? Application of fertiliser to gardens and public spaces?

Chemical fertilizers are "commonly applied" to green spaces in Southern Ontario during spring time (Hu et al., 2018). A statement clarifying this was added (Line 66).

p4, line 97: What is the shape of the a priori profile used for the retrieval? How does it compare to that from GEOS-Chem?

The a priori used at TAO is based on the a priori used at Bremen, which is based on balloon-based measurements (Toon et al., 1999). The a priori is comparable to the model profile scaled by a factor of 7. Further details of NH_3 retrieval at TAO is described in Lutsch et al. (2016).

p4, line 121: Odd to express the swath like this. Standard is as 2200 km.

2×1100 was changed to 2200 (Line 131).

p5, line 137-138: Say what model years are sampled after the one year spin up.

Fixed (Line 157).

p5, line 145-147: This approach is reasonable and widespread, but what if the spatial extent is less than the spatial resolution of IASI (at best 12 km at nadir), as seems to be the case in this work?

As suggested later in the paper, the NH_3 column from the FTIR likely has a representative scale of about ~50 km. Also, as discussed in Section 3.3, another FTIR study (Tournadre et al., 2020) found that an FTIR in Paris was capable of providing information about NH_3 variability at a ~120 km scales. For these reasons, we believe this methodology is appropriate.

Figure 2: Does the seasonality differ if the median is calculated for each month?

There are minor differences, but the general seasonality remains the same; the peak still occurs in May, and minima in January, as was the case when looking at the mean.

Figure 2: Consider showing the y-axis as 1e16 rather than 1e17.

This was fixed.

p7, line 189: Why is the seasonality solely attributed to emissions? What about partitioning of NH_3 to acidic aerosols? Is there any seasonality to this process?

The sentence was revised to "… largely due to agricultural and soil emissions increasing…". A statement about lower NH_3 columns during winter, and lower temperatures favoring NH_4SO_3 was also added (Line 209-211).

Table 1: Is there a reason that this table is included if this information is already illustrated in Figure 2?

This was included for completeness, and because while the mean column value of May was given in text, other months were not.

Table 2: The layout of the table is confusing, as the row labels correspond to specific time periods, but then the final column is labelled "during the same timeframe". What is this timeframe then? Why is the FTIR TAO trend for this same timeframe not given?

The final column gives the trends of TAO when examining data from the observational periods of NAPS and IASI. The TAO trend for "the same time period" is not given, as it would simply be itself. This was included in the table because this information is given and discussed in text. The label for this column has been changed to " TAO trends during the same timeframe as either the NAPS or IASI data".

Figure 4: The lines in (a) are not easy to see. Consider making these thicker.

Fixed.

p12, line 248: Tournadre et al. (2020) is not cited correctly.

Fixed (Line 283).

p12, line 254: What is "simple linear regression"? Ordinary least squares?

Yes, this was clarified in text (Line 288).

p12, line 259-260: It's not clear what this means: "Without temporal resampling, no significant correlation was found (r £ 0.27) for any spatial coincidence criteria". What is this temporal resampling and why does it impact the correlation?

As with the p.1 line 14 comment, the word "resampling" was changed to "averaging" to better describe what was done (Line 294).

Table 3: The information as presented in this table is okay, but would have been more visually interesting and easier to identify patterns in the data if each variable (r, slope etc.) was illustrated on 2D colored grids.

This would certainly be visually interesting, but we believe including the numbers is ultimately more important, and we have kept the table as is.

p13, line 267: What does this gridbox include other than Toronto that might dilute or increase NH3 concentrations and affect the comparison?

The gridbox contains areas near Toronto that may increase NH_3 due to agricultural emissions, as well as a significant portion of Lake Ontario, which may dilute it.

Figure 7: It would be helpful to say in the caption or text what this is showing from Table 3.

This is mentioned in text (line 287-288).

Figure 8: It is not easy to discern the red and black points in panel (b).

Figure 8b was replotted to make the points easier to discern. Due to the large number of data points, it is difficult to plot them clearly.

Figure 9: Are units for GEOS-Chem in panel (b) correct?

Yes, they are correct; the GEOS-Chem output was converted to total column values (in molecules/cm^2) to allow comparison with IASI measurements.

Multiscale observations of NH_3 around Toronto, Canada

Shoma Yamanouchi[1], Camille Viatte[2], Kimberly Strong[1], Erik Lutsch[1], Dylan B. A. Jones[1], Cathy Clerbaux[2], Martin Van Damme[3], Lieven Clarisse[3], and Pierre-Francois Coheur[3]

[1]Department of Physics, University of Toronto, Toronto, Ontario, Canada
[2]LATMOS/IPSL, Sorbonne Université, UVSQ, CNRS, Paris, France
[3]Université Libre de Bruxelles (ULB), Spectroscopy, Quantum Chemistry and Atmospheric Remote Sensing (SQUARES), Brussels, Belgium

Correspondence: Shoma Yamanouchi (syamanou@physics.utoronto.ca)

Abstract. Ammonia (NH_3) is a major source of nitrates in the atmosphere, and a major source of fine particulate matter. As such, there have been increasing efforts to measure the atmospheric abundance of NH_3 and its spatial and temporal variability. In this study, long-term measurements of NH_3 derived from multiscale datasets are examined. These NH_3 datasets include 16 years of total column measurements using Fourier transform infrared (FTIR) spectroscopy, three years of surface in-situ measurements, and 10 years of total column measurements from the Infrared Atmospheric Sounding Interferometer (IASI). The datasets were used to quantify NH_3 temporal variability over Toronto, Canada. The multiscale datasets were also compared to assess the ~~observational footprint~~ representativeness of the FTIR measurements.

All three time series showed positive trends in NH_3 over Toronto: 3.34 $\pm$ ~~0.46~~ 0.89 %/year from 2002 to 2018 in the FTIR columns, 8.88 $\pm$ ~~2.83~~ 5.08 %/year from 2013 to 2017 in the surface in-situ data, and 8.38 $\pm$ ~~0.77~~ 1.54 %/year from 2008 to 2018 in the IASI columns. To assess the ~~observational footprint~~ representative scale of the FTIR NH_3 columns, correlations between the datasets were examined. The best correlation between FTIR and IASI was obtained with coincidence criteria of $\leq$ 25 km and $\leq$ 20 minutes, with r = 0.73 and a slope of 1.14 $\pm$ 0.06. Additionally, FTIR column and in-situ measurements were standardized and correlated. Comparison of 24-day averages and monthly averages resulted in correlation coefficients of r = 0.72 and r = 0.75, respectively, although correlation without ~~resampling~~ averaging to reduce high-frequency variability led to a poorer correlation, with r = 0.39.

The GEOS-Chem model, run at 2° $\times$ 2.5° resolution, was compared against FTIR and IASI to assess model performance and investigate correlation of observational data and model output, both with local column measurements (FTIR) and measurements on a regional scale (IASI). Comparisons on a regional scale (a domain spanning 35°N to 53°N, and 93.75°W to 63.75°W) resulted in r = 0.57, and thus a coefficient of determination, which is indicative of the predictive capacity of the model, of r^2 = 0.33, but comparing a single model grid point against the FTIR resulted in a poorer correlation, with r^2 = 0.13, indicating that a finer spatial resolution is needed for modeling NH_3.

1 Introduction

Ammonia (NH_3) in the atmosphere plays an important role in the formation of nitrates and ammonium salts, is a major pollutant, and is known to be involved in numerous biochemical exchanges affecting all ecosystems (Erisman et al., 2008; Hu et al., 2014). As one of the main sources of reactive nitrogen in the atmosphere, NH_3 is also associated with acidification and eutrophication of soils and surface waters, which can negatively affect biodiversity (Vitousek et al., 1997; Krupa, 2003; Bobbink et al., 2010). Furthermore, NH_3 reacts with nitric acid and sulfuric acid to form ammonium salts, which are known to account for a large fraction of ~~particulate matter (Schaap et al., 2004; Pozzer et al., 2017). Particulate matter~~ , inorganic particulate matter (Schaap et al., 2004; Schiferl et al., 2014; Pozzer et al., 2017), and are thought to contribute to smog and haze (Liu et al., 2019; Wielgosiński and Czerwińska, 2020). Understanding how particulate matter forms is helpful in addressing air quality concerns (Schiferl et al., 2014), as particulate matter, especially that smaller than 2.5 microns ($PM_{2.5}$), ~~poses~~ pose serious health hazards ~~and is a major contributor to smog,~~ affecting life expectancy in the United States (Pope et al., 2009) and globally (Giannadaki et al., 2014).

Due to the negative impacts NH_3 can have on public health and the environment, NH_3 emissions are regulated in some parts of the world (e.g., the 1999 Gothenburg Protocol to Abate Acidification, Eutrophication and Ground-level Ozone). However, global NH_3 emissions are increasing (Warner et al., 2016; Lachatre et al., 2019), and this has been attributed to increases in agricultural livestock numbers and increased nitrogen fertilizer usage (Warner et al., 2016). In addition, as the world population continues to grow, and the demand for food rises, NH_3 emissions are expected to further increase (van Vuuren et al., 2011). Observations show increasing abundance of atmospheric NH_3, particularly in the Eastern United States, where trends as high as 12 % annually were observed (Yu et al., 2018). Yu et al. (2018) concluded that the increase in NH_3 abundance was in part due to decreasing SO_2 and ~~nitrous oxides~~NO_x ($NO + NO_2$), owing to more stringent emissions regulations. SO_2 and NO_x are precursors to acidic species (sulfuric and nitric acid, respectively) that react with NH_3, and thus their abundances in the atmosphere determine the amount of NH_3 that stays in the gaseous phase.

Atmospheric NH_3 is rapidly removed by wet and dry deposition as well as by heterogeneous reactions with acids in the atmosphere, and thus has a relatively short lifetime ranging from a few hours to a few days (Galloway et al., 2003; Dammers et al., 2019). NH_3 lifetime may be longer for certain cases, such as biomass burning emissions that inject NH_3 into the free troposphere (Höpfner et al., 2016), attenuating depositional and chemical losses, although physical and chemical mechanisms that lead to transport of NH_3 in biomass burning plumes over long distances remain uncertain (Lutsch et al., 2016, 2019). Dependence of $PM_{2.5}$ formation on NH_3 over urban areas also remains uncertain, and atmospheric chemical transport models have difficulty simulating NH_3 and $PM_{2.5}$ (e.g., Van Damme et al., 2014; Fortems-Cheiney et al., 2016; Schiferl et al., 2016; Viatte et al., 2020).

Modeled NH_3 can be used to supplement observations (Liu et al., 2017). However, ground-level NH_3 abundances are poorly modeled, due to coarse model resolution, uncertain emissions inventories, and simplification of chemistry schemes (Liu et al., 2017). Additionally, long-term trend analyses using models have been sparse (Yu et al., 2018). Representative measurements of NH_3 on both local and regional scales, as well as their spatiotemporal variabilities, are needed to better understand and model

NH_3 and $PM_{2.5}$ formation (Viatte et al., 2020).

Toronto is the most populous city in Canada, and NH_3, along with other pollutants, is monitored by several instruments. In particular, the Fourier transform infrared (FTIR) spectrometer situated at the University of Toronto Atmospheric Observatory (TAO) has been making regular measurements since 2002. It is located in downtown Toronto, where local point sources (i.e. vehicle emissions), as well as nearby agricultural emissions, are major sources of NH_3 (Zbieranowski and Aherne, 2012; Hu et al., 2014; Wentworth et al., 2014). Toronto is also regularly affected by biomass burning plumes transported from the USA and other regions of Canada (Griffin et al., 2013; Whaley et al., 2015; Lutsch et al., 2016, 2020). As such, the time series of total column NH_3 measured at TAO exhibits long-term trends and pollution episodes. Toronto also has in-situ (surface) measurements of NH_3 (Hu et al., 2014), made by Environment and Climate Change Canada. A study by Hu et al. (2014) investigating NH_3 in downtown Toronto has shown that greenery within the city, where chemical fertilizers are commonly used, is an important source of NH_3 when temperatures are above freezing, and that potential sources at temperatures below freezing have yet to be investigated. Additionally, recent studies have shown the increased capacity for satellite-based instruments to measure spatial and temporal distributions of NH_3 total columns at global (Van Damme et al., 2014; Warner et al., 2016; Shephard et al., 2020), regional (Van Damme et al., 2014; Warner et al., 2017; Viatte et al., 2020), and point-source scales (Van Damme et al., 2018; Clarisse et al., 2019a; Dammers et al., 2019).

In this study, NH_3 variability over Toronto is investigated using ground-based FTIR data, in-situ measurements, and satellite-based observations from the Infrared Atmospheric Sounding Interferometer (IASI). This study is a part of the AmmonAQ project, which investigates the role of NH_3 in air quality in urban areas. Trends in the NH_3 time series and their statistical significance are determined, and the GEOS-Chem model is also used to supplement and compare against observations. Additionally, correlations between FTIR and IASI, FTIR and in-situ, in-situ and IASI, FTIR and model data, as well as IASI and model data on a regional scale are analyzed to assess the ~~observational footprint~~ representativeness of the FTIR NH_3 measurements.

The paper is organized as follows: Section 2 describes the FTIR retrieval methodology, the in-situ and satellite data, the GEOS-Chem model, and the analysis methodologies. Section 3 presents the trend analysis of the FTIR, in-situ, and IASI measurements, the results of the correlation studies, and ~~the~~ an analysis on the representativeness of the FTIR NH_3 ~~observational footprint analysis~~. Section 4 presents the evaluation of the GEOS-Chem model, and conclusions are provided in Section 5.

2 Datasets and Methods

2.1 FTIR Measurements

Ground-based NH_3 total columns used in this study were retrieved from infrared solar absorption spectra recorded using an ABB Bomem DA8 FTIR spectrometer situated at the University of Toronto Atmospheric Observatory in downtown Toronto, Ontario, Canada (43.66°N, 79.40°W, 174 masl). This instrument has been making measurements since mid-2002, and trace gas measurements are contributed to the Network for Detection of Atmospheric Composition Change (NDACC; http://www.ndsc.ncep.noaa.gov/) (De Mazière et al., 2018). The DA8 has a maximum optical path difference of 250 cm, with a maximum

resolution of 0.004 cm^{-1}, and is equipped with a KBr (700-4300 cm^{-1}) beamsplitter. While the FTIR is equipped with both InSb and HgCdTe (MCT) detectors, NH_3 profiles were retrieved using the MCT detector, which is responsive from 500-5000 cm^{-1}. The DA8 is coupled to an active sun-tracker, which was manufactured by Aim Controls. The tracker is driven by two Shinano stepper motors on elevation and azimuth axes. The active tracking was provided by four photo-diodes from 2002-2014. This was upgraded to a camera and solar-disk-fitting system in ~~2014.~~ 2014 (Franklin, 2015). Detailed specifications of the system can be found in Wiacek et al. (2007). Due to the nature of solar-pointing FTIR spectroscopy, the measurements are limited to sunny days, resulting in gaps in the time series. Measurements are typically made on 100-150 days per year.

The ~~TAO FTIR~~ FTIR at TAO uses six filters recommended by the NDACC Infrared Working Group (IRWG), and measures spectra through each filter in sequence. NH_3 profiles were retrieved using two microwindows ~~of~~ in the 930.32-931.32 cm^{-1} and 966.97-967.675 cm^{-1} spectral regions. Interfering species include H_2O, O_3, CO_2, N_2O and HNO_3. The solar absorption spectra recorded by the DA8 were processed using the SFIT4 retrieval algorithm (https://wiki.ucar.edu/display/sfit4/). SFIT4 uses the optimal estimation method (OEM) (Rodgers, 2000), and works by iteratively adjusting the target species volume mixing ratio (VMR) profile until the difference between the calculated spectrum and the measured spectrum, and the difference between the retrieved state vector and the a priori profile is minimized. The calculated spectra use spectroscopic parameters from HITRAN 2008 (Rothman et al., 2009), and atmospheric information (temperature and pressure profiles for any particular day) provided by the US National Centers for Environmental Prediction (NCEP). A priori VMR profiles were based on the a priori used at the NDACC site in Bremen (Dammers et al., 2015), which was obtained from balloon-based measurements (Toon et al., 1999). The NH_3 retrieval methodology used at TAO is described in detail in Lutsch et al. (2016).

Uncertainties in the retrievals include measurement noise and forward model errors. Smoothing errors that arise due to the discretized vertical resolution were not included, to conform to NDACC standard practice. Measurement noise error includes errors due to uncertainties in instrument line shape, interfering species, and wavelength shifts. Uncertainties in line intensity and line widths were calculated based on HITRAN 2008 errors. Error analysis was performed on all retrievals (following Rodgers, 2000); the resulting errors were grouped into random and systematic uncertainties, and added in quadrature. The resulting mean uncertainties averaged over the entire time series, were 12.9% and 11.8% for random and systematic errors, respectively, for a total average error of 18.8% on the NH_3 total columns. The mean degrees of freedom for signal (DOFS) averaged over the 2002-2018 time series was 1.10.

2.2 In-Situ Measurements

To complement the FTIR total column NH_3 measurements, the publicly available in-situ data obtained by Environment and Climate Change Canada (ECCC) as a part of the National Air Pollution Surveillance Program (NAPS) were used (http://maps-cartes.ec.gc.ca/rnspa-naps/data.aspx)~~(National Air Pollution Surveillance Program)~~. The data span December 2013 to April 2017, with a sampling frequency of one in three days. The sampling interval is 24 hours, from 00:00 to 24:00 local time, and samples were collected with a Met One SuperSASS-Plus Sequential Speciation Sampler. The detection limit is 0.6 ppb (Yao and Zhang, 2013). The integrated samples were brought back to the lab for analysis (Yao and Zhang, 2016). While errors

are not reported in the dataset, the uncertainty is 10% when the NH_3 VMR is between 3 to 20 ppb (Hu et al., 2014). The instrument is situated less than 500 m away from the ~~TAO~~ FTIR, at 43.66°N, 79.40°W, 63 masl.

2.3 IASI Measurements

IASI is a nadir-viewing FTIR spectrometer on board the ~~Metop-A, Metop-B and Metop-C~~ MetOp-A, MetOp-B and MetOp-C polar-orbiting satellites, operated by the European Organization for the Exploitation of Meteorological Satellites (EUMETSAT), which have been operational since 2006, 2012 and 2018, respectively. ~~IASI~~ The MetOp A, B and C satellites are in the same polar orbit. For all three satellites, IASI makes measurements at 09:30 and 21:30 mean local solar time for the descending and ascending orbits. IASI records spectra in the 645-2760 cm^{-1} spectral range at a resolution of 0.5 cm^{-1}, with apodization. IASI can make off-nadir measurements up to 48.3° on either side of the track, leading to a swath of about ~~2×1100~~ 2200 km. At nadir, the ~~field-of-view is~~ field of view is a 2 × 2 ~~circular~~ matrix of pixels, each ~~at~~ with a 12 km ~~in~~ diameter (Clerbaux et al., 2009).

The IASI NH_3 total columns (IASI ANNI-NH3-v3) are retrieved using an artificial neural network retrieval algorithm, with ERA5 meteorological reanalysis input data (Van Damme et al., 2017; Franco et al., 2018). Due to this retrieval scheme, there are no averaging kernels nor vertical sensitivity information for the retrieved columns (Van Damme et al., 2014). Details of the retrieval scheme and error analysis can be found in Whitburn et al. (2016) and Van Damme et al. (2017). IASI-A and IASI-B NH_3 were combined and used in this study, as this allows for a longer time series and more data points for robust analysis. The retrieved columns of NH_3 from both satellites have been shown to be consistent with each other (Clarisse et al., 2019b; Viatte et al., 2020).

2.4 GEOS-Chem

The GEOS-Chem (v11-01) global chemical transport model (CTM) (geos-chem.org) was used in this study to supplement and compare against observational data. The model was run at 2° × 2.5° resolution (latitude × longitude) using MERRA2 (Modern-Era Retrospective analysis for Research and Applications, Version 2) meteorological fields (Molod et al., 2015), ~~the EDGAR~~ and the EDGAR v4.2 emissions database (Janssens-Maenhout et al., 2019) for anthropogenic emissions~~, and~~ . For NH_3, EDGAR v4.2 and GEIA were used as global inventories, with GEIA providing the natural source of NH_3 ~~emissions (natural and anthropogenic) provided by Bouwman et al. (1997) and Croft et al. (2016). The~~ (Bouwman et al., 1997; Olivier et al., 1998; C . The global inventories were replaced with the US EPA National Emission Inventory for 2011 (NEI11; https://www.epa.gov/air-emissions-inventories/2011-national-emissions-inventory-nei-data) in the United States, and by the Criteria Air Contaminants (CAC) from the National Pollutant Release Inventory in Canada (https://www.ec.gc.ca/inrp-npri/). The NEI11 emissions were scaled between the years 2006–2013, whereas the CAC NH_3 emissions used 2008 as the base year, with no scaling applied. The NEI11 emissions were hourly, whereas the CAC emissions were monthly. The GEOS-Chem model includes a detailed tropospheric oxidant chemistry, as well as aerosol simulation (e.g., H_2SO_4-HNO_3-NH_3 simulation) (Park et al., 2004). For SO_2 and NO, which can lead to formation of sulfates and nitrates that influence NH_3 uptake to aerosols, EDGAR and CAC (for Canada; https://www.ec.gc.ca/inrp-npri/) inventories were used. NH_3 gas-aerosol partitioning is calculated using the ISORROPIA II

model (Fountoukis and Nenes, 2007). Chemistry and transport are calculated with 20 and 10 minute timesteps, respectively. The model was spun up for one year, and output was saved every hour ~~.~~ from 2002 to 2018.

2.5 TAO FTIR and IASI Comparison

To assess the representative spatial and temporal scale of TAO FTIR NH_3 columns, the NH_3 total column measurements around Toronto made by IASI were compared against TAO FTIR total columns and modeled NH_3 columns (see Section 3.3). As NH_3 shows high spatiotemporal variability, several definitions of coincident measurements were used in this study, with spatiotemporal criteria of varying strictness. As NH_3 concentrations can vary significantly during the day, the temporal coincidence criterion was chosen to be ≤ 90 minutes (Dammers et al., 2016). In addition, values of ≤ 60, 45, 30 and 20 minutes were also tested. For spatial coincidence criteria, ≤ 25 km (Dammers et al., 2016), 30 km, 50 km, and 100 km were tested. For each criterion, correlations (both r and slope) were calculated. This analysis was used to evaluate the spatial and temporal scales represented by the TAO FTIR NH_3 columns.

2.6 Trend Analysis and Identifying Pollution Events

With 16 years of data, relatively long-term trends of TAO FTIR column time series can be examined. While a trend analysis simply using monthly averages is possible (Angelbratt et al., 2011), a more sophisticated method of fitting Fourier series of several orders was utilized in this study (Weatherhead et al., 1998). Bootstrap resampling was utilized to derive the confidence interval of the trends (Gardiner et al., 2008). A Q value (the number of bootstrap resampling ensemble members generated for statistical analysis) of 5000 was used (Gardiner et al., 2008). An additional analysis to determine the number of years of measurements needed to give the derived trend statistical significance (2σ confidence) was also conducted, following Weatherhead et al. (1998). This analysis takes into account the need for longer time series to identify trends in data that are autocorrelated (as are atmospheric observations). It should be noted that a major limitation of this analysis is that it assumes that data are collected at regular intervals, while TAO measurements are made at irregular intervals (due to the need for sunny conditions). For this reason, the confidence intervals derived from bootstrap resampling is a more robust method of error analysis, in the case of TAO data. However, as pointed out by Weatherhead et al. (1998), failing to take into account autocorrelation of the noise can lead to underestimations of actual uncertainty, and for this reason, both bootstrap resampling and the Weatherhead method were used in this study. These techniques were combined to assess the intra- and inter-annual trends of NH_3 derived from TAO measurements, including a linear trend of the NH_3 total column along with its uncertainties and statistical significance. This analysis was also applied to the NAPS in-situ and IASI data.

The Fourier fit was used to identify NH_3 enhancements, following Zellweger et al. (2009). This analysis is done by taking the negative residuals of the fit (i.e., measured values smaller than fitted values), mirroring them, and calculating the standard deviation (σ) of the mirrored residuals. Any measurements that are 2σ above the fit are considered enhancements. This analysis reduces biases in the spread due to enhancements by mirroring the negative residuals.

In this study, Fourier series of order 3 were utilized for all analyses. An analysis was done by comparing Fourier series fits of order 1 to 7, and checking for overfitting by running the residuals of the fit through a normality test (the Kolmogorov-Smirnov

test). While overfitting was not observed at higher orders, higher orders did not give more statistically-significant trends, so order 3 was chosen.

3 Results and Discussion

3.1 FTIR Measurements

The TAO FTIR total column time series of NH_3 is shown in Figure 1. The purple points indicate enhancements, and the trends (with and without outliers) are shown as red and cyan lines, respectively. The trend from 2002 to 2018 was found to be 3.34 $\pm$ ~~0.46~~ 0.89 %/year and 2.23 $\pm$ ~~0.79~~ 0.62 %/year (2σ confidence interval from bootstrap resampling), with and without outliers, respectively (see Table 2). The number of years of measurements needed for the trend to be statistically (2σ) significant was found to be 33.8 years and 29.3 years, with and without enhancement events, respectively. Due to the irregular FTIR measurement intervals, these numbers may not represent the true significance of the trends, and should be regarded as best estimates of the significance of the observed trend. The lower magnitude of the upward trend in the analysis without enhancement values indicates that the intra-annual variability of NH_3 is increasing. This is also evident when comparing the mean total column and standard deviations from, for example, the periods 2002-2005 and 2015-2018. In the former period, the mean NH_3 total column and standard deviation (1σ) were 5.94 $\pm$ 5.14 $\times 10^{15}$ molecules/cm^2, while in the latter time frame, they were 8.13 $\pm$ 7.88 $\times 10^{15}$ molecules/cm^2. The observed trend ~~at TAO~~ with the FTIR is comparable to a study by Warner et al. (2017), who observed an increasing NH_3 trend of 2.61 %/year over the United States from 2002 to 2016 using data from the Atmospheric Infrared Sounder (AIRS) satellite-based instrument.

Figure 2 shows the annual cycle of the FTIR NH_3 total columns, color coded by year, along with the monthly averages and $\pm 2\sigma$. ~~TAO~~ FTIR NH_3 columns have a maximum in May with a monthly total column average of 13.14 $\pm$ 11.69 $\times 10^{15}$ molecules/cm^2, largely due to agricultural and soil emissions increasing in spring/summer (Hu et al., 2014; Dammers et al., 2016). ~~The TAO seasonal cycle~~ , and a minimum in January with a monthly total column average of 2.11 $\pm$ 1.81 $\times 10^{15}$ molecules/cm^2. The lower NH_3 columns during winter months may be due to lower temperatures favoring the formation of NH_4NO_3 (Li et al., 2014). The seasonal cycle observed with the FTIR is consistent with findings by Van Damme et al. (2015b), who observed maximum NH_3 columns over the central United States during March-April-May (MAM). The mean NH_3 total column across the entire FTIR time series was 7.53 $\pm$ 7.10 $\times 10^{15}$ molecules/cm^2. These values are higher than remote areas, such as Eureka (located at 80.05°N, 86.42°W), where the highest monthly average was 0.279 $\times 10^{15}$ molecules/cm^2, in July (Lutsch et al., 2016). However, ~~TAO~~ the TAO FTIR NH_3 total columns are far below values observed by the FTIR in Bremen (located at 53.10°N, 8.85°E), which saw values in the range of $\sim$100 $\times 10^{15}$ molecules/cm^2 (Dammers et al., 2016). Monthly mean NH_3 columns are listed in Table 1.

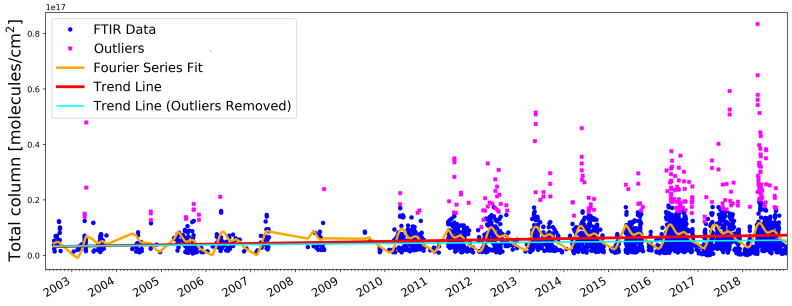

Figure 1. Time series of TAO FTIR NH_3 total columns from 2002 to 2018 with third-order Fourier series fit and linear trends.

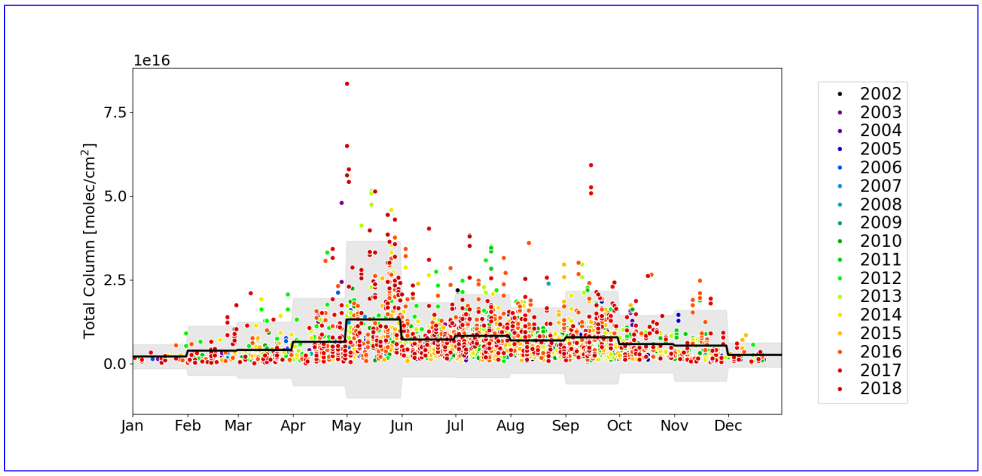

Figure 2. TAO FTIR NH_3 total columns plotted from January to December for 2002 to 2018. Monthly averages and $\pm$ 2σ are indicated by the black line and shading, respectively.

3.2 NAPS Measurements

The NAPS in-situ NH_3 time series is shown in Figure 3. The purple points indicate enhancements, and trendlines with and without these outliers are shown as the red and cyan lines, respectively. The trendline was found to have a slope of 8.88 $\pm$ ~~2.83~~ 5.08 %/year and 6.40 $\pm$ ~~0.18~~ 4.37 %/year (2σ confidence interval from bootstrap resampling), with and without outliers, respectively. The number of years needed for this trend to be 2σ significant was 8.4 years for both. Since NAPS data have very regular measurement intervals (once every three days), they are well suited for this trend significance analysis. Given that NAPS data only spans 3 years and 5 months, and 8.4 years of measurements are needed for 2σ confidence in the observed trend, it is uncertain if the increase in NH_3 levels is a definitive trend. For comparison, analysis of TAO FTIR NH_3 total columns during the same time period resulted in trends of 9.31 $\pm$ ~~2.86~~ 5.73 %/year and 7.42 $\pm$ ~~0.38~~ 4.48 %/year, with and without outliers, respectively.

Table 1. Monthly mean (1σ in parenthesis) NH_3 total columns ~~at~~ of the TAO FTIR (2002-2018).

Month	Mean Columns ($\times 10^{15}$ molecules/cm^2)
January	2.11 (1.81)
February	3.84 (3.68)
March	4.05 (4.19)
April	6.48 (6.52)
May	13.14 (11.69)
June	7.17 (5.54)
July	8.27 (6.19)
August	6.89 (4.89)
September	7.81 (6.91)
October	5.81 (4.30)
November	5.36 (5.28)
December	2.59 (1.81)
Overall Mean	7.53 (7.10)

Table 2. Comparison of NH_3 trends and 2σ confidence intervals observed in Toronto. All trends are in %/year.

Dataset	Timeframe	Trends	Trends without outliers	~~TAO trends during the same timeframe~~ TAO trends during the same timeframe as either the NAPS or IASI data
TAO	2002-2018	$3.34 \pm$ ~~0.46~~ 0.89	$2.23 \pm$ ~~0.79~~ 0.62	-
NAPS	2013-2017	$8.88 \pm$ ~~2.83~~ 5.08	$6.40 \pm$ ~~0.18~~ 4.37	$9.31 \pm$ ~~2.86~~ 5.73
IASI	2008-2018	$8.38 \pm$ ~~0.77~~ 1.54	-	$4.02 \pm$ ~~0.74~~ 1.42

The in-situ NH_3 VMRs were compared against the TAO FTIR columns by standardizing both measurements, following Equation 1 of Viatte et al. (2020):

$$X^i_{\text{standardized}} = \frac{X_i - \mu_X}{\sigma_X} \tag{1}$$

where X is the dataset, indexed by i, μ is the mean, and σ is the standard deviation of the dataset. The standardized dataset is centered around zero, and normalized by the standard deviation of the measurements. As the standardized dataset is unitless, it allows for comparison between different measurements in different units. In this study, the TAO FTIR NH_3 total columns were used, because the DOFS for the retrieval was around 1 (mean DOFS of the entire time series was 1.10), meaning there is only about one piece of vertical information in these measurements.

Standardized ~~TAO~~ FTIR and NAPS NH_3 are plotted in Figure 4a. Monthly averages and monthly standard deviations are

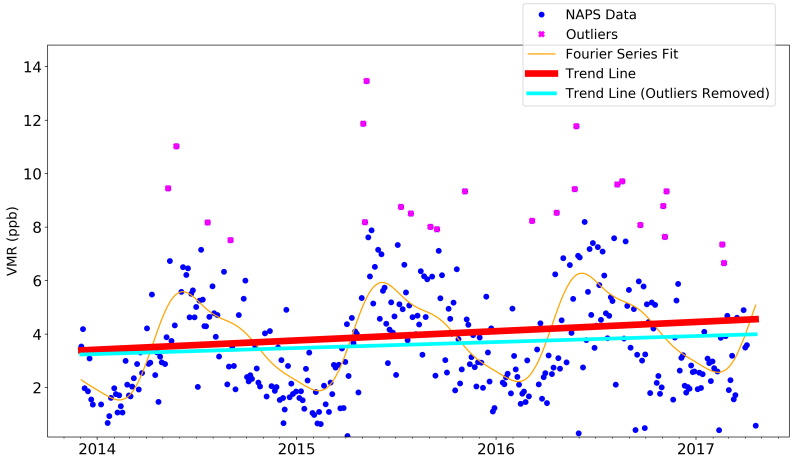

Figure 3. Time series of NAPS NH_3 surface VMR from 2013 to 2017 with third-order Fourier series fit and linear trends.

shown in Figure 4b. The two measurements show similar seasonal cycles, with a maximum in May, and a minimum in December and January. There is a smaller secondary peak in November for both measurements. This may be due to late-season fertilizer application and cover crop growth. The Ministry of Agriculture, Food and Rural Affairs of Ontario recommends applying fertilizer in spring and fall (Munroe et al., 2018). Correlation between the two datasets can be seen in Figure 5a, where each NAPS measurement is plotted against the average of ~~TAO~~ FTIR measurements on that day (if any measurements are available). This simple comparison does not show a strong correlation, with r = 0.51, and slope = 0.501. However, resampling the measurements by 15-day averages (Figure 5b), 18-day averages (Figure 5c), 24-day averages (Figure 5d) and by monthly averages (Figure 5e), show much stronger correlations. Resampling to 15-day averages show better correlation with r = 0.63, and a larger slope = 0.707. Averaging to every 18 days and 24 days leads to r = 0.68 and 0.72, respectively. Monthly averages show the highest correlation with r = 0.75, and a slope = 0.758. This indicates that ~~TAO~~ the FTIR and NAPS see similar low-frequency variabilities (period of 2 weeks or longer) in NH_3.

It should be noted that a bias would be expected to be observed between the FTIR and NAPS data, as the FTIR can only make measurements during sunny conditions, while NAPS data are 24-hour averages, made once every three days. This means that NAPS data include observations made during nighttime and rainy conditions. This is noteworthy, as surface NH_3 concentrations may be affected by diurnal variability in the planetary boundary layer height. Temperature may also affect NH_3 enhancement events. When coincident datasets were analyzed for enhancements, three days showed simultaneous enhancements (25 May 2014, 23 May 2016, 26 May 2016). On all three days, the daily average temperature (measured by the TAO weather station) was higher than the corresponding monthly average: 19.3 $\pm$ 2.8 °C (uncertainties indicate 1 standard deviation) on 25 May 2014 vs. May 2014 monthly mean of 13.8 °C, and 19.6 $\pm$ 3.4 and 21.2 $\pm$ 2.8 °C for 23 May and 26 May 2016, respectively, vs. the May 2016 monthly mean of 14.1 °C. This is unsurprising, given that increased NH_3 is correlated with higher temperatures

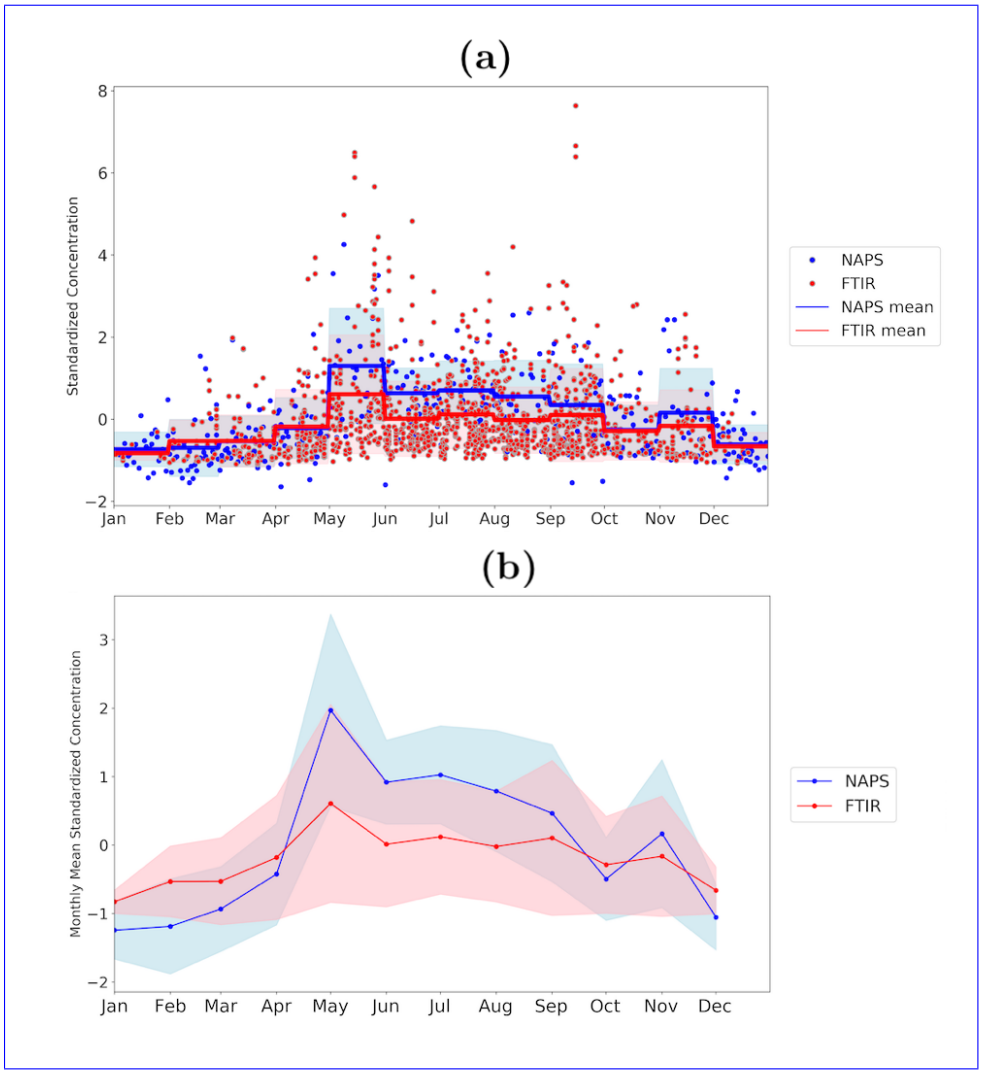

Figure 4. (a) Standardized ~~TAO~~ FTIR total column and NAPS surface VMR of NH_3 plotted from January to December. Monthly averages and $\pm$ 1σ are indicated by the red and blue lines and shading for ~~TAO~~ the FTIR and NAPS, respectively. (b) The standardized ~~TAO~~ FTIR NH_3 total column (red) and NAPS surface NH_3 VMR (blue) monthly averages lines with their respective $\pm$ 1σ (shading).

(e.g., Meng et al., 2011). Since the FTIR can only make measurements on sunny days, its measurements may be biased high compared to NAPS, which makes measurements regardless of weather.

3.3 IASI Measurements

260 The time series of IASI NH_3 total columns (2008 to 2018) within 50 km of TAO is shown in Figure 6. The trend of these IASI measurements is 8.38 $\pm$ ~~0.77~~ 1.43 %/year, where the error indicates the 2σ confidence interval obtained by bootstrap resampling analysis. The Weatherhead et al. (1998) method for finding the statistical significance of this trend was not utilized

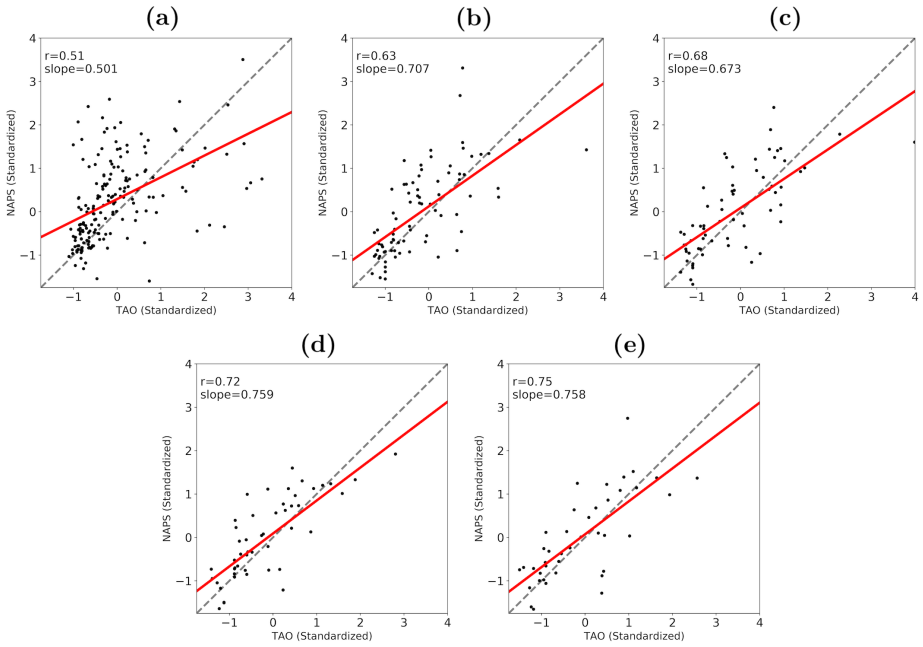

Figure 5. Standardized NAPS NH_3 surface VMR plotted against standardized ~~TAO~~ FTIR NH_3 total column. (a) The raw comparison, where for each NAPS observation, the closest daily average ~~TAO~~ FTIR measurement, if there are any within 72 hours, is plotted. ~~TAO~~ FTIR and in-situ resampled to (b) 15-day, (c) 18-day, (d) 24-day and (e) monthly averages. The dashed lines indicate slope = 1, and the red lines indicate the fit to the data.

here, as the analysis requires calculating the autocorrelation of data, which is not possible given the spatially scattered dataset. For comparison, the TAO FTIR trend over the same period is 4.02 $\pm$ ~~0.74~~ 1.42 %/year.

The correlations between IASI and TAO FTIR NH_3 columns for the various coincidence criteria listed in Section 2.3 are shown in Table 3, along with the slopes, mean relative difference (MRD), and total number of data points. The MRD was calculated by subtracting the TAO FTIR column from the IASI column, then dividing by the TAO FTIR column (Dammers et al., 2016). To maximize the number of coincident data points, no significant data filtering (e.g., filtering by relative errors) was performed. The criteria used by Dammers et al. (2016) (90 minutes, 25 km) shows a correlation with r = 0.65 and slope = 0.88 in this study, comparable to r = 0.79 and slope = 0.84 reported by Dammers et al. (2016). The MRD was -45.5 $\pm$ 207.2 % for this study, consistent with -46.0 $\pm$ 47.0 % calculated by Dammers et al. (2016) for TAO FTIR data. The larger standard deviation of the MRD is most likely because the data used here were not filtered by relative errors. The best correlation was achieved when using measurements made within 20 minutes and within 25 km of each other, which resulted in r = 0.73 and slope of 1.14. Coincidence criteria of 20 minutes and 50 km gave r = 0.68 and slope = 1.06. Criteria of 45 minutes and 50 km also shows a correlation comparable to the 90 minutes, 25 km criteria, with r = 0.64 and slope = 0.92. This suggests that TAO FTIR is a good indicator of NH_3 concentrations on a city-wide scale ($\sim$ 50 km). This is also evident when looking at the correlation between TAO FTIR columns vs. daily averaged IASI measurements within 50 km, which had r =

0.69, although the slope was smaller, at 0.82. The better correlations seen with the stricter temporal criteria suggest that NH_3 near Toronto exhibits high-frequency variability. The values obtained in this study are also comparable to recent findings by Tournadre et al. (2020), who compared NH_3 columns from an FTIR stationed in Paris to IASI NH_3 columns. With a 15 km and 30 minutes coincidence criteria, the FTIR in Paris showed a correlation of r = 0.79 and slope = 0.73. The same study also found that the FTIR in Paris is capable of providing information about NH_3 variability at a "regional" scale ($\sim$ 120 km) ~~Tournadre et al. (2020)~~(Tournadre et al., 2020). Although not quantified in this study, the line-of-sight through the atmosphere (which changes throughout the day) may also affect the representative scale of ground-based solar-pointing FTIR observations. Additionally, the number of observations is relatively large for each criterion (e.g., N = 923 for 90 minutes, 25 km, while N = 679 for 45 minutes, 50 km), suggesting that the differences in correlation are not simply due to the differences in the number of data points. The correlation plots for 20 min/25 km, 90 min/25 km, 20 min/50 km and 45 min/50 km are shown in Figures 7a, 7b, 7c and 7d, respectively. It should be noted that the slope was calculated through a simple linear least-squares regression. For comparison, an additional analysis was done propagating measurement uncertainty using the unified least squares procedure outlined by York et al. (2004) and yielded similar results, with a smaller slope for all cases due to the larger relative uncertainty on IASI measurements ($\sim$68 % for IASI compared to $\sim$19 % for TAO FTIR).

IASI column and NAPS surface NH_3 were also compared in this study by converting to standardized data (see Equation 1). Comparing the monthly means resulted in r = 0.79 and slope = 0.79 when looking at IASI measurements made within 50 km of NAPS, and r = 0.74 and slope = 0.74 for 30 km. Without temporal ~~resampling~~averaging, no significant correlation was found ($r \leq 0.27$) for any spatial coincidence criteria. This is in line with findings from Van Damme et al. (2015a), where significant correlation was found when comparing monthly averaged surface and IASI measurements. Van Damme et al. (2015a) report r = 0.28 when comparing IASI with an ensemble of surface observations over Europe, and r as high as 0.81 and 0.71 for measurements made at Fyodorovskoye, Russia and the Monte Bondone, Italy, respectively. It should be noted that the comparisons in Van Damme et al. (2015a) were done by converting IASI NH_3 columns to surface concentration by using the same model used in the retrieval process, as opposed to the standardized dataset approach used in this study.

4 Comparison with GEOS-Chem

The NH_3 total column from the GEOS-Chem CTM model grid cell containing Toronto (grid center at 44°N, 80°W) is shown in Figure 8a, along with TAO FTIR data. The correlation was obtained by comparing the hourly model data for each FTIR observation. Comparison with the FTIR was done with and without smoothing the model data with the FTIR averaging kernel and a priori profile (Rodgers and Connor, 2003). As smoothing the model data only resulted in differences of less than 1%, the discussion here will focus on the unsmoothed dataset to be consistent with the comparison with IASI. While GEOS-Chem is able to capture the seasonal cycle seen ~~at TAO~~with the FTIR, the correlation is not strong, with r = 0.51 and the coefficient of determination, r^2, at 0.26 (see Figure 9a). The calculated slope was 1.16. Both of these values are without smoothing the model data. Smoothing the data resulted in r^2 = 0.28, and slope = 1.01 It is likely that the model is too coarse (the 2° $\times$ 2.5° grid box corresponds to approximately 220 km $\times$ 200 km), and ~~TAO~~the FTIR, while able to capture larger-scale variability in

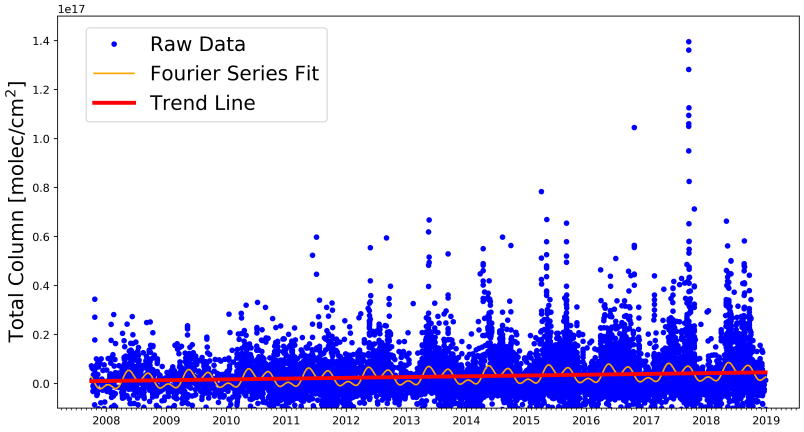

Figure 6. Time series of IASI NH_3 total columns measured within 50 km of TAO. The third-order Fourier series fit and the trend line are shown in orange and red, respectively.

NH_3 than in-situ observations, is not sensitive to observations at spatial scales of 100 km or larger. Given the short lifetime of NH_3, it is unsurprising to see large variability at these spatial scales.

For comparison with IASI, a larger domain was chosen to assess the correlation of the model and satellite observations at a larger regional scale. Model grids spanning 35°N to 53°N, and 93.75°W to 63.75°W were used for the analysis, as these grids capture Toronto, the Great Lakes, and the Atlantic Ocean coastline. The spatial coincidence was calculated by binning the IASI data into the grids of GEOS-Chem, and temporal coincidence was determined by calculating the mean overpass time in the domain and averaging the model data between one hour before and one hour after the mean overpass time. The time series (both GEOS-Chem and IASI were averaged over the domain) and correlation plots are shown in Figures 8b and 9b, respectively. Correlation of GEOS-Chem against IASI is higher than GEOS-Chem against TAO FTIR, with r^2 = 0.33 ~~.~~ (see Figure 9b). Removing enhancement events from observational data led to poorer correlation with GEOS-Chem, with r^2 = 0.22 and r^2 = 0.29 for the FTIR and IASI, respectively (see Figures 9c and 9d). This is comparable to findings by Schiferl et al. (2016), who observed IASI and GEOS-Chem correlations (r) of 0.6–0.8 in the United States Great Plains and the Midwest during the summer. The slope was 0.85, meaning NH_3 is overestimated in GEOS-Chem when compared to IASI at this scale. Comparing GEOS-Chem and IASI for one grid cell over Toronto (same cell as the one used for comparison with TAO FTIR) resulted in a lower correlation, at r^2 = 0.13. These results suggest GEOS-Chem is able to model NH_3 on larger regional scales, but a finer resolution is needed for better comparison with smaller regions. In addition, while the modeled NH_3 was overestimated in comparison with IASI over a larger regional domain, the comparison for the single grid box over Toronto resulted in slope = 2.44, meaning the model underestimated NH_3 in this smaller region, which may indicate underestimation of local NH_3 sources near Toronto in the model. This can be contrasted to recent findings by Van Damme et al. (2014), who observed an overall underestimation of NH_3 in the LOTOS-EUROS model over Europe when compared against IASI. In a four-year period from

Table 3. IASI vs. TAO FTIR correlation coefficient, slope (regression standard error in parenthesis), MRD (1σ RMS in parenthesis) (in %), and number of data points, calculated for each TAO FTIR measurement, for varying spatial and temporal coincidence criteria.

Coincidence criteria	$\leq$ 25 km	$\leq$ 30 km	$\leq$ 50 km	$\leq$ 100 km
$\leq$ 20 minutes	r = 0.73 slope = 1.14 (0.06) MRD = -61.9 (161.6) % N = 314	r = 0.72 slope = 1.11 (0.06) MRD = -58.3 (156.7) % N = 337	r = 0.68 slope = 1.06 (0.06) MRD = -51.2 (166.1) % N = 384	r = 0.63 slope = 1.24 (0.08) MRD = -47.7 (190.9) % N = 421
$\leq$ 30 minutes	r = 0.71 slope = 1.06 (0.05) MRD = -48.1 (216.8) % N = 438	r = 0.70 slope = 1.04 (0.05) MRD = -43.1 (204.2) % N = 470	r = 0.65 slope = 0.98 (0.05) MRD = -42.0 (200.4) % N = 528	r = 0.59 slope = 1.07 (0.06) MRD = -40.9 (186.7) % N = 575
$\leq$ 45 minutes	r = 0.68 slope = 0.93 (0.04) MRD = -47.4 (198.2) % N = 588	r = 0.67 slope = 0.92 (0.04) MRD = -42.8 (190.6) % N = 623	r = 0.64 slope = 0.92 (0.04) MRD = -41.0 (185.5) % N = 679	r = 0.58 slope = 0.97 (0.05) MRD = -42.4 (177.9) % N = 732
$\leq$ 60 minutes	r = 0.66 slope = 0.89 (0.04) MRD = -46.4 (188.4) % N = 708	r = 0.65 slope = 0.90 (0.04) MRD = -42.8 (180.3) % N = 750	r = 0.62 slope = 0.89 (0.04) MRD = -38.2 (176.7) % N = 815	r = 0.56 slope = 0.93 (0.05) MRD = -40.7 (172.1) % N = 866
$\leq$ 90 minutes	r = 0.65 slope = 0.88 (0.03) MRD = -45.5 (207.2) % N = 923	r = 0.65 slope = 0.88 (0.03) MRD = -44.1 (192.4) % N = 967	r = 0.61 slope = 0.89 (0.04) MRD = -40.7 (193.5) % N = 1039	r = 0.56 slope = 0.93 (0.04) MRD = -36.9 (186.3) % N = 1093

2008 to 2011 over the Netherlands, for example, IASI NH_3 columns are as high as 6.5 mg/m^2, while the modeled NH_3 go up to 5.2 mg/m^2 (Van Damme et al., 2014).

5 Conclusions

The ~~TAO~~ FTIR spectrometer situated in downtown Toronto, Ontario, Canada has been used to obtain a 16-year time series of total columns of NH_3. These columns were compared against other NH_3 observations (IASI column and NAPS in-situ surface VMR) and GEOS-Chem model data. Analysis of ~~TAO~~ the FTIR NH_3 columns showed an upward annual trend of 3.34 $\pm$ ~~0.46~~ 0.89 % and 2.23 $\pm$ ~~0.79~~ 0.62 % over the period 2002-2018, with and without outliers, respectively. The larger trend with outliers included~~suggests~~ , along with a larger variance in the total column measurements in the later years, suggest that NH_3 enhancements are becoming more frequent and seasonal variability is increasing. These values are in agreement with trends observed by other studies. For example, Warner et al. (2017) observed a trend of 2.61 %/year from 2002 to 2016 over the

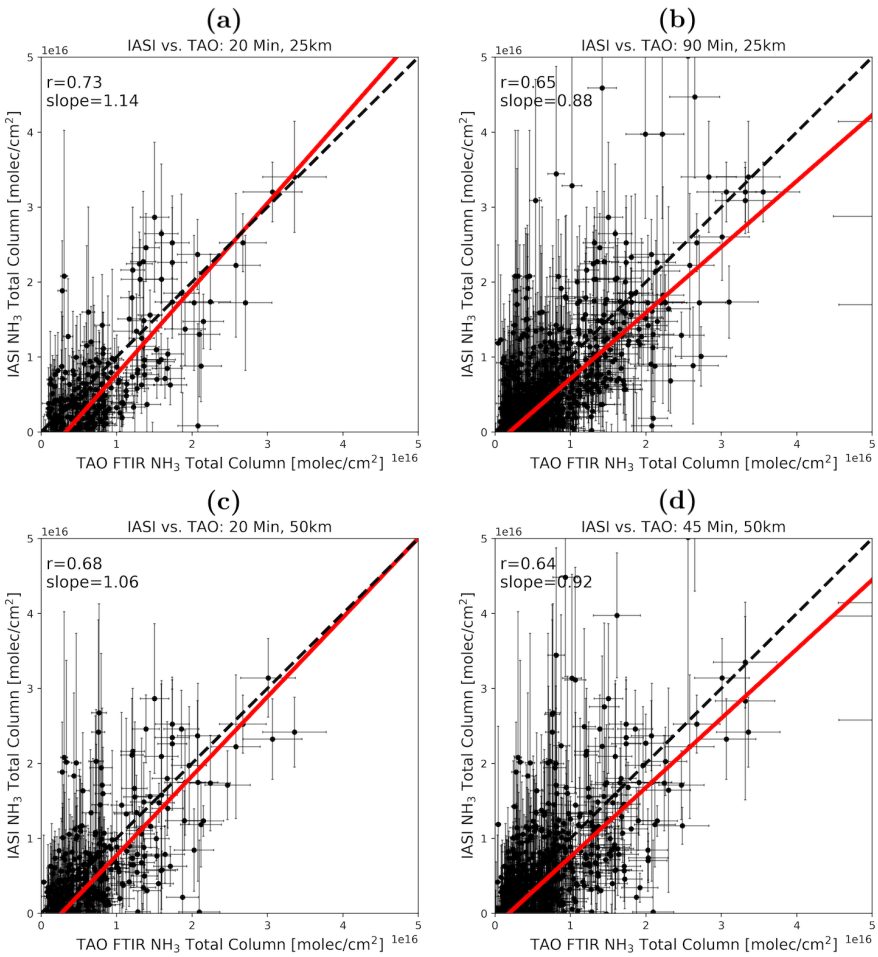

Figure 7. Correlation plots for IASI vs. TAO FTIR NH_3 total columns, with coincidence criteria of (a) 20 minutes and 25 km, (b) 90 minutes and 25 km, (c) 20 minutes and 50 km, and (d) 45 minutes and 50 km. Data from 2008 to 2018 are plotted. Dashed lines indicate slope = 1, while the red lines are the lines of best fit. Error bars are the reported observational uncertainties.

USA using data from the Atmospheric Infrared Sounder (AIRS) aboard NASA's Aqua satellite, and Yu et al. (2018) derived surface NH_3 trends of ∼5 % and ∼5-12 % in the Western and Eastern United States from 2001 to 2016, respectively, using GEOS-Chem modeled NH_3.

Similar analysis of the NAPS in-situ time series showed that NH_3 at the surface is also increasing, with an annual increase of 8.88 ± ~~2.83~~ 5.08 % and 6.40 ± ~~0.18~~ 4.37 % calculated with and without outliers, respectively. ~~TAO~~ The FTIR total columns during the same period showed trends of 9.31 ± ~~2.86~~ 5.73 %/year and 7.42 ± ~~0.38~~ 4.48 %/year with and without outliers, respectively. ~~TAO~~ The FTIR and NAPS comparisons showed that ~~TAO~~ the FTIR columns are well correlated with surface NH_3 when resampled to monthly means to reduce high-frequency variability.

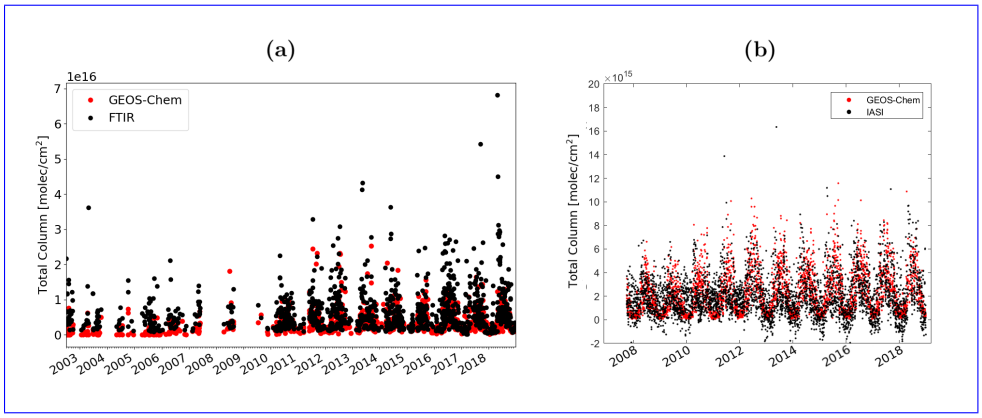

Figure 8. (a) GEOS-Chem and TAO FTIR NH_3 total columns from 2002 to 2018. GEOS-Chem data shown here were not smoothed with the FTIR averaging kernel and a priori profile. (b) GEOS-Chem and IASI NH_3 total columns (averaged over domain spanning from 35°N to 53°N, and 93.75°W to 63.75°W) from 2008 to 2018.

IASI NH_3 total columns measured within 50 km of TAO exhibited an annual trend of 8.38 ± ~~0.77~~ 1.54 %/year from 2008 to 2018. For comparison, TAO FTIR NH_3 total columns over the same period showed a trend of 4.02 ± ~~0.74~~ 1.42 %/year. The IASI columns were also compared against FTIR columns, with the good correlations being obtained with distance criterion of ∼50 km, indicating that the TAO FTIR measurements are representative of NH_3 at a city-size scale. Comparing different coincidence criteria showed that, at least in Toronto, distance criteria can be larger than the 25 km used by Dammers et al. (2016), but temporal criteria may need to be stricter, at around ∼45 minutes (instead of 90 minutes). The highest correlation (r = 0.73) was seen with coincidence criteria of 25 km and 20 minutes.

TAO FTIR and IASI NH_3 columns were also compared with GEOS-Chem model data. The model did not show a very high correlation with ~~TAO~~ the TAO FTIR for a single grid cell containing Toronto, with r^2 = 0.26, and r^2 = 0.28 when the model data was smoothed with the FTIR averaging kernel. The model comparison with IASI showed slightly better agreement on a domain spanning 35°N to 53°N, and 93.75°W to 63.75°W, with r^2 = 0.33. These results suggest that TAO FTIR, representative of NH_3 at a city-size scale (∼50 km), requires higher-resolution model runs for comparison. This is also evident when comparing GEOS-Chem against IASI within the single model grid cell that includes TAO; this comparison led to a poorer correlation with r^2 = 0.13. In addition, GEOS-Chem overestimated NH_3 in the larger domain when compared with IASI. However, in the single grid cell over TAO, the model underestimated NH_3 columns compared to both IASI and TAO FTIR.

This study showed a positive trend of NH_3 over Toronto derived from ground-based FTIR, satellite, and in-situ measurements. The NH_3 total columns using an FTIR situated in downtown Toronto ~~showed an observational footprint at~~ are representative of a city-size scale, although this also highlights the need for models simulating NH_3 to be run at higher resolution than 2° × 2.5° for comparisons with ground-based measurements.

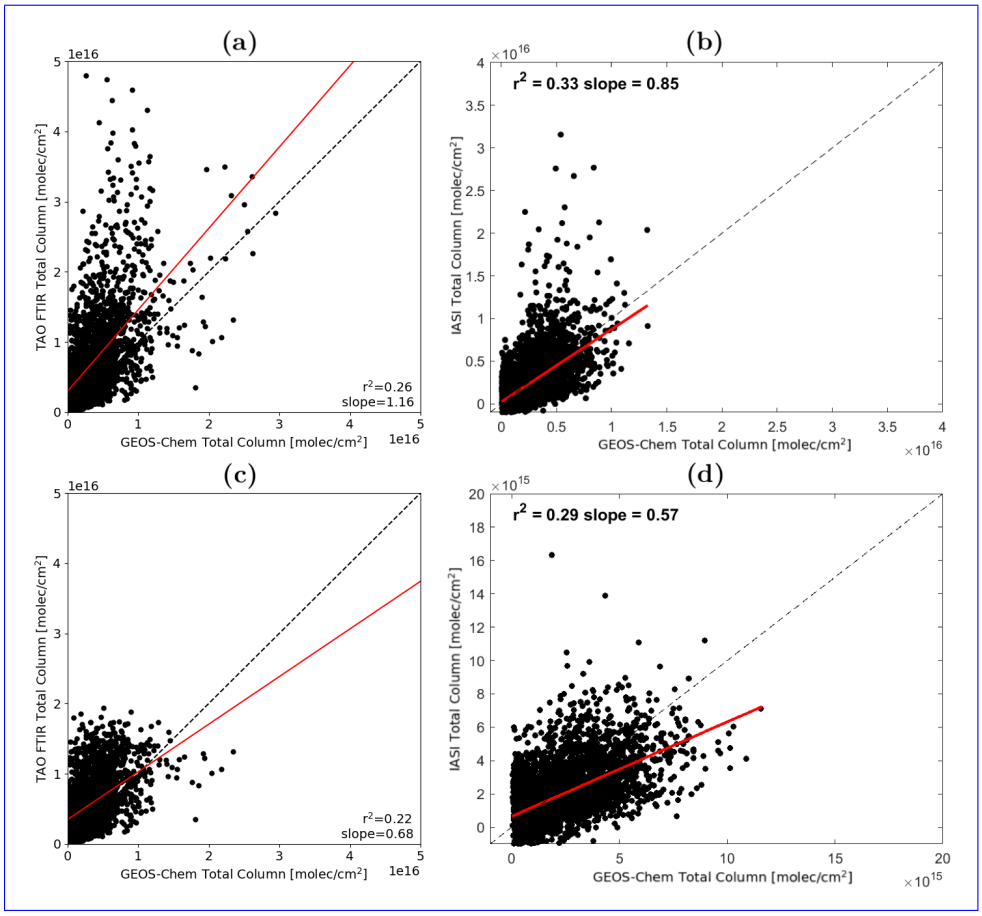

Figure 9. Correlation plots of (a) TAO FTIR vs. GEOS-Chem NH_3 total columns, ~~and~~ (b) IASI vs. GEOS-Chem NH_3 total columns (c) TAO FTIR with enhancement events removed vs. GEOS-Chem NH_3 total columns, and (d) IASI with enhancement events removed vs. GEOS-Chem NH_3 total columns. Data from 2002 to 2018 are plotted for TAO and data from 2008 to 2018 are plotted for IASI.

Data availability. The TAO FTIR data used in this study are publicly available from the NDACC data repository hosted by NOAA at ftp://ftp.cpc.ncep.noaa.gov/ndacc/station/toronto/hdf/ftir/. The IASI ANNI-NH3-v3 data used in this study are available on request (M. Van Damme, ULB). The IASI Level-1C data are distributed in near real time by Eumetsat through the EumetCast system distribution. IASI Level-1C data and Level-2 NH_3 data can be accessed via the Aeris data infrastructure (http://iasi.aeris-data.fr/NH3/). The in-situ NH_3 data measured by the Canadian National Air Pollution Surveillance (NAPS) are available at http://data.ec.gc.ca/data/air/monitor/national-air-pollution-surveillance-naps-program/, provided by Environment and Climate Change Canada (last access: November 2019) (National Air Pollution Surveillance Program). The GEOS-Chem model (v11-01) is freely available to the public. Latest model information can be found at The International GEOS-Chem User Community (2020). Instructions for downloading and running the models can be found at http://wiki.geos-chem.org/.

Author contributions. SY, CV and KS conceived this study. SY wrote the paper with contributions from all authors. EL and SY performed the retrieval of NH_3 columns at TAO. SY ran the GEOS-Chem model with guidance from DBAJ. SY and CV performed the analyses and comparisons of NH_3 measurements around Toronto. MVD, LC, and SW performed IASI retrievals, and CV analyzed the IASI retrievals with guidance from CC and PFC. All of the authors discussed the results and contributed to the final paper.

Competing interests. No competing interests are present.

Acknowledgements. This project was made possible thanks to the 2018 Centre National de la Recherche Scientifique – University of Toronto Call for Joint Research Proposals, which provided the initial support for the AmmonAQ project. This work, including measurements made at TAO, was supported by Environment and Climate Change Canada (ECCC), the Natural Sciences and Engineering Research Council (NSERC), and the NSERC CREATE Training Program in Technologies for Exo-Planetary Science. IASI is a joint mission of EUMETSAT and the Centre National d'Etudes Spatiales (CNES, France). The authors acknowledge the Aeris data infrastructure (http://iasi.aeris-data.fr/NH3/) for providing access to the IASI data, as well as ECCC for the NAPS in-situ data. ULB has been supported by the Belgian State Federal Office for Scientific, Technical and Cultural Affairs (Prodex arrangement IASI.FLOW). LC and MVD are respectively research associate and postdoctoral researcher with the Belgian F.R.S-FNRS.

References

Angelbratt, J., Mellqvist, J., Blumenstock, T., Borsdorff, T., Brohede, S., Duchatelet, P., Forster, F., Hase, F., Mahieu, E., Murtagh, D., Petersen, A. K., Schneider, M., Sussmann, R., and Urban, J.: A new method to detect long term trends of methane (CH_4) and nitrous oxide (N_2O) total columns measured within the NDACC ground-based high resolution solar FTIR network, Atmospheric Chemistry and Physics, 11, 6167–6183, https://doi.org/10.5194/acp-11-6167-2011, https://www.atmos-chem-phys.net/11/6167/2011/, 2011.

Bobbink, R., Hicks, K., Galloway, J., Spranger, T., Alkemade, R., Ashmore, M., Bustamante, M., Cinderby, S., Davidson, E., Dentener, F., Emmett, B., Erisman, J.-W., Fenn, M., Gilliam, F., Nordin, A., Pardo, L., and De Vries, W.: Global assessment of nitrogen deposition effects on terrestrial plant diversity: a synthesis, Ecological Applications, 20, 30–59, https://doi.org/10.1890/08-1140.1, https://esajournals.onlinelibrary.wiley.com/doi/abs/10.1890/08-1140.1, 2010.

Bouwman, A. F., Lee, D. S., Asman, W. A. H., Dentener, F. J., Van Der Hoek, K. W., and Olivier, J. G. J.: A global high-resolution emission inventory for ammonia, Global Biogeochemical Cycles, 11, 561–587, https://doi.org/10.1029/97GB02266, https://agupubs.onlinelibrary.wiley.com/doi/abs/10.1029/97GB02266, 1997.

Clarisse, L., Van Damme, M., Clerbaux, C., and Coheur, P.-F.: Tracking down global NH_3 point sources with wind-adjusted superresolution, Atmospheric Measurement Techniques, 12, 5457–5473, https://doi.org/10.5194/amt-12-5457-2019, https://www.atmos-meas-tech.net/12/5457/2019/, 2019a.

Clarisse, L., Van Damme, M., Gardner, W., Coheur, P.-F., Clerbaux, C., Whitburn, S., Hadji-Lazaro, J., and Hurtmans, D.: Atmospheric ammonia (NH_3) emanations from Lake Natron's saline mudflats, Scientific Reports, 9, 4441–4452, https://doi.org/10.1038/s41598-019-39935-3, https://doi.org/10.1038/s41598-019-39935-3, 2019b.

Clerbaux, C., Boynard, A., Clarisse, L., George, M., Hadji-Lazaro, J., Herbin, H., Hurtmans, D., Pommier, M., Razavi, A., Turquety, S., Wespes, C., and Coheur, P.-F.: Monitoring of atmospheric composition using the thermal infrared IASI/MetOp sounder, Atmospheric Chemistry and Physics, 9, 6041–6054, https://doi.org/10.5194/acp-9-6041-2009, https://www.atmos-chem-phys.net/9/6041/2009/, 2009.

Croft, B., Wentworth, G. R., Martin, R. V., Leaitch, W. R., Murphy, J. G., Murphy, B. N., Kodros, J. K., Abbatt, J. P. D., and Pierce, J. R.: Contribution of Arctic seabird-colony ammonia to atmospheric particles and cloud-albedo radiative effect, Nature Communications, 7, 13 444, https://doi.org/10.1038/ncomms13444, 2016.

Dammers, E., Vigouroux, C., Palm, M., Mahieu, E., Warneke, T., Smale, D., Langerock, B., Franco, B., Van Damme, M., Schaap, M., Notholt, J., and Erisman, J. W.: Retrieval of ammonia from ground-based FTIR solar spectra, Atmospheric Chemistry and Physics, 15, 12 789–12 803, https://doi.org/10.5194/acp-15-12789-2015, https://www.atmos-chem-phys.net/15/12789/2015/, 2015.

Dammers, E., Palm, M., Van Damme, M., Vigouroux, C., Smale, D., Conway, S., Toon, G. C., Jones, N., Nussbaumer, E., Warneke, T., Petri, C., Clarisse, L., Clerbaux, C., Hermans, C., Lutsch, E., Strong, K., Hannigan, J. W., Nakajima, H., Morino, I., Herrera, B., Stremme, W., Grutter, M., Schaap, M., Wichink Kruit, R. J., Notholt, J., Coheur, P.-F., and Erisman, J. W.: An evaluation of IASI-NH_3 with ground-based Fourier transform infrared spectroscopy measurements, Atmospheric Chemistry and Physics, 16, 10 351–10 368, https://doi.org/10.5194/acp-16-10351-2016, https://www.atmos-chem-phys.net/16/10351/2016/, 2016.

Dammers, E., McLinden, C. A., Griffin, D., Shephard, M. W., Van Der Graaf, S., Lutsch, E., Schaap, M., Gainairu-Matz, Y., Fioletov, V., Van Damme, M., Whitburn, S., Clarisse, L., Cady-Pereira, K., Clerbaux, C., Coheur, P. F., and Erisman, J. W.: NH_3 emissions from large point sources derived from CrIS and IASI satellite observations, Atmospheric Chemistry and Physics, 19, 12 261–12 293, https://doi.org/10.5194/acp-19-12261-2019, https://www.atmos-chem-phys.net/19/12261/2019/, 2019.

De Mazière, M., Thompson, A. M., Kurylo, M. J., Wild, J. D., Bernhard, G., Blumenstock, T., Braathen, G. O., Hannigan, J. W., Lambert, J.-C., Leblanc, T., McGee, T. J., Nedoluha, G., Petropavlovskikh, I., Seckmeyer, G., Simon, P. C., Steinbrecht, W., and Strahan, S. E.: The Network for the Detection of Atmospheric Composition Change (NDACC): history, status and perspectives, Atmospheric Chemistry and Physics, 18, 4935–4964, https://doi.org/10.5194/acp-18-4935-2018, https://www.atmos-chem-phys.net/18/4935/2018/, 2018.

Erisman, J. W., Sutton, M. A., Galloway, J., Klimont, Z., and Winiwarter, W.: How a century of ammonia synthesis changed the world, Nature Geoscience, 1, 636–639, https://doi.org/10.1038/ngeo325, https://doi.org/10.1038/ngeo325, 2008.

Fortems-Cheiney, A., Dufour, G., Hamaoui-Laguel, L., Foret, G., Siour, G., Van Damme, M., Meleux, F., Coheur, P.-F., Clerbaux, C., Clarisse, L., Favez, O., Wallasch, M., and Beekmann, M.: Unaccounted variability in NH_3 agricultural sources detected by IASI contributing to European spring haze episode, Geophysical Research Letters, 43, 5475–5482, https://doi.org/10.1002/2016GL069361, https://agupubs.onlinelibrary.wiley.com/doi/abs/10.1002/2016GL069361, 2016.

Fountoukis, C. and Nenes, A.: ISORROPIA II: a computationally efficient thermodynamic equilibrium model for K^+-Ca^{2+}-Mg^{2+}-$NH_4{}^+$-Na^+-$SO_4{}^{2-}$-$NO_3{}^-$-Cl^--H_2O aerosols, Atmospheric Chemistry and Physics, 7, 4639–4659, https://doi.org/10.5194/acp-7-4639-2007, https://www.atmos-chem-phys.net/7/4639/2007/, 2007.

Franco, B., Clarisse, L., Stavrakou, T., Müller, J.-F., Van Damme, M., Whitburn, S., Hadji-Lazaro, J., Hurtmans, D., Taraborrelli, D., Clerbaux, C., and Coheur, P.-F.: A General Framework for Global Retrievals of Trace Gases From IASI: Application to Methanol, Formic Acid, and PAN, Journal of Geophysical Research: Atmospheres, 123, 13,963–13,984, https://doi.org/10.1029/2018JD029633, 2018.

Franklin, J.: Solar Absorption Spectroscopy at the Dalhousie Atmospheric Observatory, Ph.D. thesis, Dalhousie University, Halifax, Nova Scotia, Canada, 2015.

Galloway, J. N., Aber, J. D., Erisman, J. W., Seitzinger, S. P., Howarth, R. W., Cowling, E. B., and Cosby, B. J.: The Nitrogen Cascade, BioScience, 53, 341–356, https://doi.org/10.1641/0006-3568(2003)053[0341:TNC]2.0.CO;2, https://doi.org/10.1641/0006-3568(2003)053[0341:TNC]2.0.CO;2, 2003.

Gardiner, T., Forbes, A., de Mazière, M., Vigouroux, C., Mahieu, E., Demoulin, P., Velazco, V., Notholt, J., Blumenstock, T., Hase, F., Kramer, I., Sussmann, R., Stremme, W., Mellqvist, J., Strandberg, A., Ellingsen, K., and Gauss, M.: Trend analysis of greenhouse gases over Europe measured by a network of ground-based remote FTIR instruments, Atmospheric Chemistry and Physics, 8, 6719–6727, https://doi.org/10.5194/acp-8-6719-2008, https://www.atmos-chem-phys.net/8/6719/2008/, 2008.

Giannadaki, D., Pozzer, A., and Lelieveld, J.: Modeled global effects of airborne desert dust on air quality and premature mortality, Atmospheric Chemistry and Physics, 14, 957–968, https://doi.org/10.5194/acp-14-957-2014, https://www.atmos-chem-phys.net/14/957/2014/, 2014.

Griffin, D., Walker, K. A., Franklin, J. E., Parrington, M., Whaley, C., Hopper, J., Drummond, J. R., Palmer, P. I., Strong, K., Duck, T. J., Abboud, I., Bernath, P. F., Clerbaux, C., Coheur, P.-F., Curry, K. R., Dan, L., Hyer, E., Kliever, J., Lesins, G., Maurice, M., Saha, A., Tereszchuk, K., and Weaver, D.: Investigation of CO, C_2H_6 and aerosols in a boreal fire plume over eastern Canada during BORTAS 2011 using ground- and satellite-based observations and model simulations, Atmospheric Chemistry and Physics, 13, 10 227–10 241, https://doi.org/10.5194/acp-13-10227-2013, https://www.atmos-chem-phys.net/13/10227/2013/, 2013.

Höpfner, M., Volkamer, R., Grabowski, U., Grutter, M., Orphal, J., Stiller, G., von Clarmann, T., and Wetzel, G.: First detection of ammonia (NH_3) in the Asian

summer monsoon upper troposphere, Atmospheric Chemistry and Physics, 16, 14 357–14 369, https://doi.org/10.5194/acp-16-14357-2016, https://acp.copernicus.org/articles/16/14357/2016/, 2016.

Hu, Q., Zhang, L., Evans, G. J., and Yao, X.: Variability of atmospheric ammonia related to potential emission sources in downtown Toronto, Canada, Atmospheric Environment, 99, 365 – 373, https://doi.org/https://doi.org/10.1016/j.atmosenv.2014.10.006, http://www.sciencedirect.com/science/article/pii/S1352231014007833, 2014.

Janssens-Maenhout, G., Crippa, M., Guizzardi, D., Muntean, M., Schaaf, E., Dentener, F., Bergamaschi, P., Pagliari, V., Olivier, J. G. J., Peters, J. A. H. W., van Aardenne, J. A., Monni, S., Doering, U., Petrescu, A. M. R., Solazzo, E., and Oreggioni, G. D.: EDGAR v4.3.2 Global Atlas of the three major greenhouse gas emissions for the period 1970–2012, Earth System Science Data, 11, 959–1002, https://doi.org/10.5194/essd-11-959-2019, https://www.earth-syst-sci-data.net/11/959/2019/, 2019.

Krupa, S.: Atmosphere and agriculture in the new millennium, Environmental Pollution, 126, 293 – 300, https://doi.org/https://doi.org/10.1016/S0269-7491(03)00242-2, http://www.sciencedirect.com/science/article/pii/S0269749103002422, 2003.

Lachatre, M., Fortems-Cheiney, A., Foret, G., Siour, G., Dufour, G., Clarisse, L., Clerbaux, C., Coheur, P.-F., Van Damme, M., and Beekmann, M.: The unintended consequence of SO_2 and NO_2 regulations over China: increase of ammonia levels and impact on $PM_{2.5}$ concentrations, Atmospheric Chemistry and Physics, 19, 6701–6716, https://doi.org/10.5194/acp-19-6701-2019, https://www.atmos-chem-phys.net/19/6701/2019/, 2019.

Li, Y., Schwandner, F. M., Sewell, H. J., Zivkovich, A., Tigges, M., Raja, S., Holcomb, S., Molenar, J. V., Sherman, L., Archuleta, C., Lee, T., and Collett, J. L.: Observations of ammonia, nitric acid, and fine particles in a rural gas production region, Atmospheric Environment, 83, 80 – 89, https://doi.org/https://doi.org/10.1016/j.atmosenv.2013.10.007, http://www.sciencedirect.com/science/article/pii/S1352231013007607, 2014.

Liu, L., Zhang, X., Xu, W., Liu, X., Lu, X., Wang, S., Zhang, W., and Zhao, L.: Ground Ammonia Concentrations over China Derived from Satellite and Atmospheric Transport Modeling, Remote Sensing, 9, 247, https://doi.org/10.3390/rs9050467, https://www.mdpi.com/2072-4292/9/5/467, 2017.

Liu, M., Huang, X., Song, Y., Tang, J., Cao, J., Zhang, X., Zhang, Q., Wang, S., Xu, T., Kang, L., Cai, X., Zhang, H., Yang, F., Wang, H., Yu, J. Z., Lau, A. K. H., He, L., Huang, X., Duan, L., Ding, A., Xue, L., Gao, J., Liu, B., and Zhu, T.: Ammonia emission control in China would mitigate haze pollution and nitrogen deposition, but worsen acid rain, Proceedings of the National Academy of Sciences, 116, 7760–7765, https://doi.org/10.1073/pnas.1814880116, 2019.

~~Lutsch, E.,~~ Lutsch, E., Dammers, ~~E.,~~ E., Conway, ~~S., and Strong, K.:~~ S., and Strong, K.: Long-range ~~transport of NH~~transport of NH_3, ~~CO, HCN, and C~~CO, HCN, and C_2H_6 from the 2014 Canadian Wildfires, Geophysical Research Letters, 43, 8286–8297, ~~,~~ https://doi.org/10.1002/2016GL070114, https://agupubs.onlinelibrary.wiley.com/doi/abs/10.1002/2016GL070114, 2016.

~~Lutsch, E., Strong, K., Jones, D.B. A., Blumenstock, T., Conway, S., Fisher, J. A., Hannigan, J. W., Hase, F., Kasai, Y., Mahieu, E., Makarova, M., Morino, I., Nagahama, T., Notholt, J., Ortega, I., Palm, M., Poberovskii, A. V., Sussmann, R., and Warneke, T.: Detection and Attribution of Wildfire Pollution in the Arctic and Northern Mid-latitudes using a Network of FTIR Spectrometers and GEOS-Chem, Atmospheric Chemistry and Physics Discussions, 2019, 1–57, , , 2019.~~

Lutsch, E., Strong, K., Jones, D. B. A., Ortega, I., Hannigan, J. W., Dammers, E., Shephard, M. W., Morris, E., Murphy, K., Evans, M. J., Parrington, M., Whitburn, S., Van Damme, M., Clarisse, L., Coheur, P.-F., Clerbaux, C., Croft, B., Martin, R. V., Pierce, J. R., and Fisher,

J. A.: Unprecedented Atmospheric Ammonia Concentrations Detected in the High Arctic From the 2017 Canadian Wildfires, Journal of Geophysical Research: Atmospheres, 124, 8178–8202, https://doi.org/10.1029/2019JD030419, ~~2019.~~2019.

Lutsch, E., Strong, K., Jones, D. B. A., Blumenstock, T., Conway, S., Fisher, J. A., Hannigan, J. W., Hase, F., Kasai, Y., Mahieu, E., Makarova, M., Morino, I., Nagahama, T., Notholt, J., Ortega, I., Palm, M., Poberovskii, A. V., Sussmann, R., and Warneke, T.: Detection and attribution of wildfire pollution in the Arctic and northern midlatitudes using a network of Fourier-transform infrared spectrometers and GEOS-Chem, Atmospheric Chemistry and Physics, 20, 12 813–12 851, https://doi.org/10.5194/acp-20-12813-2020, 2020.

Meng, Z. Y., Lin, W. L., Jiang, X. M., Yan, P., Wang, Y., Zhang, Y. M., Jia, X. F., and Yu, X. L.: Characteristics of atmospheric ammonia over Beijing, China, Atmospheric Chemistry and Physics, 11, 6139–6151, https://doi.org/10.5194/acp-11-6139-2011, 2011.

Molod, A., Takacs, L., Suarez, M., and Bacmeister, J.: Development of the GEOS-5 atmospheric general circulation model: evolution from MERRA to MERRA2, Geoscientific Model Development, 8, 1339–1356, https://doi.org/10.5194/gmd-8-1339-2015, https://www.geosci-model-dev.net/8/1339/2015/, 2015.

Munroe, J., Brown, C., Kessel, C., Verhallen, A., Lauzon, J., O'Halloran, I., Bruulsema, T., and Cowan, D.: Soil Fertility Handbook Publication 611, Ministry of Agriculture, Food and Rural Affairs (OMAFRA), 3 edn., http://www.omafra.gov.on.ca/english/crops/pub611/pub611.pdf, 2018.

National Air Pollution Surveillance Program: (Last accessed: November 2019). Available from the Government of Canada Open Data Portal at https://open.canada.ca/data/en/dataset/1b36a356-defd-4813-acea-47bc3abd859b.

Olivier, J., Bouwman, A., Van der Hoek, K., and Berdowski, J.: Global air emission inventories for anthropogenic sources of NOx, NH3 and N2O in 1990, Environmental Pollution, 102, 135 – 148, https://doi.org/https://doi.org/10.1016/S0269-7491(98)80026-2, http://www.sciencedirect.com/science/article/pii/S0269749198800262, nitrogen, the Confer-N-s First International Nitrogen Conference 1998, 1998.

Park, R. J., Jacob, D. J., Field, B. D., Yantosca, R. M., and Chin, M.: Natural and transboundary pollution influences on sulfate-nitrate-ammonium aerosols in the United States: Implications for policy, Journal of Geophysical Research: Atmospheres, 109, https://doi.org/10.1029/2003JD004473, https://agupubs.onlinelibrary.wiley.com/doi/abs/10.1029/2003JD004473, 2004.

Pope, C. A., Ezzati, M., and Dockery, D. W.: Fine-Particulate Air Pollution and Life Expectancy in the United States, New England Journal of Medicine, 360, 376–386, https://doi.org/10.1056/NEJMsa0805646, https://doi.org/10.1056/NEJMsa0805646, pMID: 19164188, 2009.

Pozzer, A., Tsimpidi, A. P., Karydis, V. A., de Meij, A., and Lelieveld, J.: Impact of agricultural emission reductions on fine-particulate matter and public health, Atmospheric Chemistry and Physics, 17, 12 813–12 826, https://doi.org/10.5194/acp-17-12813-2017, https://www.atmos-chem-phys.net/17/12813/2017/, 2017.

Rodgers, C. D.: Inverse Methods for Atmospheric Sounding, chap. 5, p. 81–100, WORLD SCIENTIFIC, https://doi.org/10.1142/3171, https://www.worldscientific.com/doi/abs/10.1142/3171, 2000.

Rodgers, C. D. and Connor, B. J.: Intercomparison of remote sounding instruments, Journal of Geophysical Research: Atmospheres, 108, https://doi.org/10.1029/2002JD002299, https://agupubs.onlinelibrary.wiley.com/doi/abs/10.1029/2002JD002299, 2003.

Rothman, L., Gordon, I., Barbe, A., Benner, D., Bernath, P., Birk, M., Boudon, V., Brown, L., Campargue, A., Champion, J.-P., Chance, K., Coudert, L., Dana, V., Devi, V., Fally, S., Flaud, J.-M., Gamache, R., Goldman, A., Jacquemart, D., Kleiner, I., Lacome, N., Lafferty, W., Mandin, J.-Y., Massie, S., Mikhailenko, S., Miller, C., Moazzen-Ahmadi, N., Naumenko, O., Nikitin, A., Orphal, J., Perevalov, V., Perrin, A., Predoi-Cross, A., Rinsland, C., Rotger, M., Šimečková, M., Smith, M., Sung, K., Tashkun, S., Tennyson, J., Toth, R., Vandaele, A., and Auwera, J. V.: The HITRAN 2008 molecular spectroscopic database, Journal of Quantitative Spectroscopy and Radiative Transfer, 110, 533 – 572, https://doi.org/https://doi.org/10.1016/j.jqsrt.2009.02.013, http://www.sciencedirect.com/science/article/pii/S0022407309000727, hITRAN, 2009.

Schaap, M., van Loon, M., ten Brink, H. M., Dentener, F. J., and Builtjes, P. J. H.: Secondary inorganic aerosol simulations for Europe with special attention to nitrate, Atmospheric Chemistry and Physics, 4, 857–874, https://doi.org/10.5194/acp-4-857-2004, https://www.atmos-chem-phys.net/4/857/2004/, 2004.

Schiferl, L. D., Heald, C. L., Nowak, J. B., Holloway, J. S., Neuman, J. A., Bahreini, R., Pollack, I. B., Ryerson, T. B., Wiedinmyer, C., and Murphy, J. G.: An investigation of ammonia and inorganic particulate matter in California during the CalNex campaign, Journal of Geophysical Research: Atmospheres, 119, 1883–1902, https://doi.org/10.1002/2013JD020765, 2014.

Schiferl, L. D., Heald, C. L., Van Damme, M., Clarisse, L., Clerbaux, C., Coheur, P.-F., Nowak, J. B., Neuman, J. A., Herndon, S. C., Roscioli, J. R., and Eilerman, S. J.: Interannual variability of ammonia concentrations over the United States: sources and implications, Atmospheric Chemistry and Physics, 16, 12 305–12 328, https://doi.org/10.5194/acp-16-12305-2016, https://www.atmos-chem-phys.net/16/12305/2016/, 2016.

Shephard, M. W., Dammers, E., Cady-Pereira, K. E., Kharol, S. K., Thompson, J., Gainariu-Matz, Y., Zhang, J., McLinden, C. A., Kovachik, A., Moran, M., Bittman, S., Sioris, C. E., Griffin, D., Alvarado, M. J., Lonsdale, C., Savic-Jovcic, V., and Zheng, Q.: Ammonia measurements from space with the Cross-track Infrared Sounder: characteristics and applications, Atmospheric Chemistry and Physics, 20, 2277–2302, https://doi.org/10.5194/acp-20-2277-2020, https://www.atmos-chem-phys.net/20/2277/2020/, 2020.

The International GEOS-Chem User Community: geoschem/geos-chem: GEOS-Chem 12.9.2, https://doi.org/10.5281/zenodo.3959279, https://doi.org/10.5281/zenodo.3959279, v12.9.2. Please see the LICENSE.txt and AUTHORS.txt files in the root folder for the GEOS-Chem license description (based on the MIT license) and a complete list of authors. For more information about GEOS-Chem in general, please see www.geos- chem.org and wiki.geos-chem.org., 2020.

Toon, G. C., Blavier, J.-F., Sen, B., Margitan, J. J., Webster, C. R., May, R. D., Fahey, D., Gao, R., Del Negro, L., Proffitt, M., Elkins, J., Romashkin, P. A., Hurst, D. F., Oltmans, S., Atlas, E., Schauffler, S., Flocke, F., Bui, T. P., Stimpfle, R. M., Bonne, G. P., Voss, P. B., and Cohen, R. C.: Comparison of MkIV balloon and ER-2 aircraft measurements of atmospheric trace gases, Journal of Geophysical Research: Atmospheres, 104, 26 779–26 790, https://doi.org/10.1029/1999JD900379, https://agupubs.onlinelibrary.wiley.com/doi/abs/10.1029/1999JD900379, 1999.

Tournadre, B., Chelin, P., Ray, M., Cuesta, J., Kutzner, R. D., Landsheere, X., Fortems-Cheiney, A., Flaud, J.-M., Hase, F., Blumenstock, T., Orphal, J., Viatte, C., and Camy-Peyret, C.: Atmospheric ammonia (NH_3) over the Paris megacity: 9 years of total column observations from ground-based infrared remote sensing, Atmospheric Measurement Techniques, 13, 3923–3937, https://doi.org/10.5194/amt-13-3923-2020, https://amt.copernicus.org/articles/13/3923/2020/, 2020.

Van Damme, M., Clarisse, L., Heald, C. L., Hurtmans, D., Ngadi, Y., Clerbaux, C., Dolman, A. J., Erisman, J. W., and Coheur, P. F.: Global distributions, time series and error characterization of atmospheric ammonia (NH_3) from IASI satellite observations, Atmospheric Chemistry and Physics, 14, 2905–2922, https://doi.org/10.5194/acp-14-2905-2014, https://www.atmos-chem-phys.net/14/2905/2014/, 2014.

Van Damme, M., Clarisse, L., Dammers, E., Liu, X., Nowak, J. B., Clerbaux, C., Flechard, C. R., Galy-Lacaux, C., Xu, W., Neuman, J. A., Tang, Y. S., Sutton, M. A., Erisman, J. W., and Coheur, P. F.: Towards validation of ammonia (NH_3) measurements from the IASI satellite, Atmospheric Measurement Techniques, 8, 1575–1591, https://doi.org/10.5194/amt-8-1575-2015, https://www.atmos-meas-tech.net/8/1575/2015/, 2015a.

Van Damme, M., Erisman, J. W., Clarisse, L., Dammers, E., Whitburn, S., Clerbaux, C., Dolman, A. J., and Coheur, P.-F.: Worldwide spatiotemporal atmospheric ammonia (NH3) columns variability revealed by satellite, Geophysical Research Letters, 42, 8660–8668, https://doi.org/10.1002/2015GL065496, https://agupubs.onlinelibrary.wiley.com/doi/abs/10.1002/2015GL065496, 2015b.

Van Damme, M., Whitburn, S., Clarisse, L., Clerbaux, C., Hurtmans, D., and Coheur, P.-F.: Version 2 of the IASI NH_3 neural network retrieval algorithm: near-real-time and reanalysed datasets, Atmospheric Measurement Techniques, 10, 4905–4914, https://doi.org/10.5194/amt-10-4905-2017, https://www.atmos-meas-tech.net/10/4905/2017/, 2017.

Van Damme, M., Clarisse, L., Whitburn, S., Hadji-Lazaro, J., Hurtmans, D., Clerbaux, C., and Coheur, P.-F.: Industrial and agricultural ammonia point sources exposed, Atmospheric Chemistry and Physics, 564, 99–103, https://doi.org/10.1038/s41586-018-0747-1, 2018.

van Vuuren, D. P., Edmonds, J., Kainuma, M., Riahi, K., Thomson, A., Hibbard, K., Hurtt, G. C., Kram, T., Krey, V., Lamarque, J.-F., Masui, T., Meinshausen, M., Nakicenovic, N., Smith, S. J., and Rose, S. K.: The representative concentration pathways: an overview, Climatic Change, 109, 5, https://doi.org/10.1007/s10584-011-0148-z, https://doi.org/10.1007/s10584-011-0148-z, 2011.

Van Damme, M., Wichink Kruit, R., Schaap, M., Clarisse, L., Clerbaux, C., Coheur, P.-F., Dammers, E., Dolman, A., and Erisman, J.: Evaluating 4 years of atmospheric ammonia (NH3) over Europe using IASI satellite observations and LOTOS-EUROS model results, Journal of Geophysical Research: Atmospheres, 119, 9549–9566, https://doi.org/10.1002/2014JD021911, https://agupubs.onlinelibrary.wiley.com/doi/abs/10.1002/2014JD021911, 2014.

Viatte, C., Wang, T., Van Damme, M., Dammers, E., Meleux, F., Clarisse, L., Shephard, M. W., Whitburn, S., Coheur, P. F., Cady-Pereira, K. E., and Clerbaux, C.: Atmospheric ammonia variability and link with particulate matter formation: a case study over the Paris area, Atmospheric Chemistry and Physics, 20, 577–596, https://doi.org/10.5194/acp-20-577-2020, https://www.atmos-chem-phys.net/20/577/2020/, 2020.

Vitousek, P. M., Mooney, H. A., Lubchenco, J., and Melillo, J. M.: Human Domination of Earth's Ecosystems, Science, 277, 494–499, https://doi.org/10.1126/science.277.5325.494, https://science.sciencemag.org/content/277/5325/494, 1997.

Warner, J. X., Wei, Z., Strow, L. L., Dickerson, R. R., and Nowak, J. B.: The global tropospheric ammonia distribution as seen in the 13-year AIRS measurement record, Atmospheric Chemistry and Physics, 16, 5467–5479, https://doi.org/10.5194/acp-16-5467-2016, https://www.atmos-chem-phys.net/16/5467/2016/, 2016.

Warner, J. X., Dickerson, R. R., Wei, Z., Strow, L. L., Wang, Y., and Liang, Q.: Increased atmospheric ammonia over the world's major agricultural areas detected from space, Geophysical Research Letters, 44, 2875–2884, https://doi.org/10.1002/2016GL072305, https://agupubs.onlinelibrary.wiley.com/doi/abs/10.1002/2016GL072305, 2017.

Weatherhead, E. C., Reinsel, G. C., Tiao, G. C., Meng, X.-L., Choi, D., Cheang, W.-K., Keller, T., DeLuisi, J., Wuebbles, D. J., Kerr, J. B., Miller, A. J., Oltmans, S. J., and Frederick, J. E.: Factors affecting the detection of trends: Statistical considerations and applications to environmental data, Journal of Geophysical Research: Atmospheres, 103, 17 149–17 161, https://doi.org/10.1029/98JD00995, https://agupubs.onlinelibrary.wiley.com/doi/abs/10.1029/98JD00995, 1998.

Wentworth, G. R., Murphy, J. G., Gregoire, P. K., Cheyne, C. A. L., Tevlin, A. G., and Hems, R.: Soil–atmosphere exchange of ammonia in a non-fertilized grassland: measured emission potentials and inferred fluxes, Biogeosciences, 11, 5675–5686, https://doi.org/10.5194/bg-11-5675-2014, https://www.biogeosciences.net/11/5675/2014/, 2014.

Whaley, C. H., Strong, K., Jones, D. B. A., Walker, T. W., Jiang, Z., Henze, D. K., Cooke, M. A., McLinden, C. A., Mittermeier, R. L., Pommier, M., and Fogal, P. F.: Toronto area ozone: Long-term measurements and modeled sources of poor air quality events, Journal of Geophysical Research: Atmospheres, 120, 11,368–11,390, https://doi.org/10.1002/2014JD022984, https://agupubs.onlinelibrary.wiley.com/doi/abs/10.1002/2014JD022984, 2015.

Whitburn, S., Van Damme, M., Clarisse, L., Bauduin, S., Heald, C. L., Hadji-Lazaro, J., Hurtmans, D., Zondlo, M. A., Clerbaux, C., and Coheur, P.-F.: A flexible and robust neural network IASI-NH3 retrieval algorithm, Journal of Geophysical Research: Atmospheres, 121, 6581–6599, https://doi.org/10.1002/2016JD024828, https://agupubs.onlinelibrary.wiley.com/doi/abs/10.1002/2016JD024828, 2016.

Wiacek, A., Taylor, J. R., Strong, K., Saari, R., Kerzenmacher, T. E., Jones, N. B., and Griffith, D. W. T.: Ground-Based Solar Absorption FTIR Spectroscopy: Characterization of Retrievals and First Results from a Novel Optical Design Instrument at a New NDACC Complementary Station, Journal of Atmospheric and Oceanic Technology, 24, 432–448, https://doi.org/10.1175/JTECH1962.1, https://doi.org/10.1175/JTECH1962.1, 2007.

Wielgosiński, G. and Czerwińska, J.: Smog Episodes in Poland, Atmosphere, 11, 277, https://doi.org/10.3390/atmos11030277, 2020.

Yao, X. and Zhang, L.: Trends in atmospheric ammonia at urban, rural, and remote sites across North America, Atmospheric Chemistry and Physics, 16, 11 465–11 475, https://doi.org/10.5194/acp-16-11465-2016, https://www.atmos-chem-phys.net/16/11465/2016/, 2016.

Yao, X. H. and Zhang, L.: Analysis of passive-sampler monitored atmospheric ammonia at 74 sites across southern Ontario, Canada, Biogeosciences, 10, 7913–7925, https://doi.org/10.5194/bg-10-7913-2013, https://www.biogeosciences.net/10/7913/2013/, 2013.

York, D., Evensen, N. M., Martinez, M. L., and De Basabe Delgado, J.: Unified equations for the slope, intercept, and standard errors of the best straight line, American Journal of Physics, 72, 367–375, https://doi.org/10.1119/1.1632486, https://doi.org/10.1119/1.1632486, 2004.

Yu, F., Nair, A. A., and Luo, G.: Long-Term Trend of Gaseous Ammonia Over the United States: Modeling and Comparison With Observations, Journal of Geophysical Research: Atmospheres, 123, 8315–8325, https://doi.org/10.1029/2018JD028412, https://agupubs.onlinelibrary.wiley.com/doi/abs/10.1029/2018JD028412, 2018.

Zbieranowski, A. L. and Aherne, J.: Ambient concentrations of atmospheric ammonia, nitrogen dioxide and nitric acid across a rural–urban–agricultural transect in southern Ontario, Canada, Atmospheric Environment, 62, 481 – 491, https://doi.org/https://doi.org/10.1016/j.atmosenv.2012.08.040, http://www.sciencedirect.com/science/article/pii/S1352231012008126, 2012.

Zellweger, C., Hüglin, C., Klausen, J., Steinbacher, M., Vollmer, M., and Buchmann, B.: Inter-comparison of four different carbon monoxide measurement techniques and evaluation of the long-term carbon monoxide time series of Jungfraujoch, Atmospheric Chemistry and Physics, 9, 3491–3503, https://doi.org/10.5194/acp-9-3491-2009, https://www.atmos-chem-phys.net/9/3491/2009/, 2009.